Proton-Coupled Electron Transfer and Tyrosine D of Photosystem II

A Dissertation
Presented to
The Academic Faculty

By

David L. Jenson

In Partial Fulfillment
Of the Requirements for the Degree
Doctor of Philosophy in the
School of Chemistry and Biochemistry

Georgia Institute of Technology

August, 2009

Proton-Coupled Electron Transfer and Tyrosine D of Photosystem II

Approved by:

Dr. Bridgette Barry, Advisor
School of Chemistry and Biochemistry
Georgia Institute of Technology

Dr. Ingeborg Schmidt-Krey
School of Biology
Georgia Institute of Technology

Dr. Wendy Kelly
School of Chemistry and Biochemistry
Georgia Institute of Technology

Dr. Jake Soper
School of Chemistry and Biochemistry
Georgia Institute of Technology

Dr. Nils Kröger
School of Chemistry and Biochemistry
Georgia Institute of Technology

Date Approved: May 6, 2009

Table of Contents

List of Tables

Chapter 1

Chapter 2

Chapter 3

Chapter 4

List of Figures

Chapter 1

Chapter 2

Chapter 3

Chapter 4

List of Schemes

Chapter 1

Chapter 2

Chapter 3

Chapter 4

List of Symbols and Abbreviations

ATR	Attenuated Total Reflectance
Chl	Chlorophyll
CPET	Coupled proton-electron transfer
D1	Reaction center binding polypeptide of PSII
D2	Reaction center binding polypeptide of PSII
DCBQ	2,6-dichlorobenzoquinone
DCMU	3-(3,4-dichlorophenyl)-1,1dimethylurea
EPR	Electron paramagnetic resonance
ESE-ENDOR	Electron spin echo-electron nuclear double resonance
ESEEM	Electron spin-echo envelope modulation
ET	Electron Transfer
ETPT	Electron transfer-proton transfer
FT-IR	Fourier transform infrared
HEPES	4-(2-hydroxyethyl)-1-piperazineethanesulfonic acid
KIE	Kinetic isotope effect
kDa	Kilodalton
L_2O	Lyonium oxide
MES	2-(*N*-morpholino)ethanesulfonic acid
NaOL	Sodium lyoxide
Nd:YAG	Neodymium:yttrium aluminum garnet
OEC	Oxygen evolving complex
PCET	Proton-coupled electron transfer
PSII	Photosystem II
PTET	Proton transfer-electron transfer
Q_A	Plastoquinone A
Q_B	Plastoquinone B
Tris	Tris(hydroxymethyl)aminomethane
Y_D	Tyrosine D; Tyrosine 161 of the D2 polypeptide in PSII
$Y_D^{\bullet}$	Tyrosine D radical

Y_Z	Tyrosine Z; Tyrosine 160 of the D1 polypeptide in PSII
$Y_Z^{\bullet}$	Tyrosine Z radical
ϕ_R	Reactant state fractionation factor
ϕ_T	Transition state fractionation factor

Special Note on the Symbolic Representation of the Tyrosyl Radical

1) The neutral tyrosyl radical is represented throughout by the following structure:

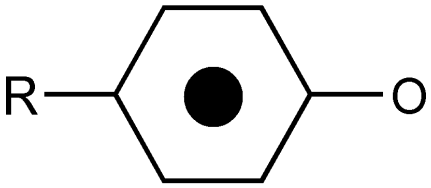

2) The cationic tyrosyl radical is represented throughout by the following structure:

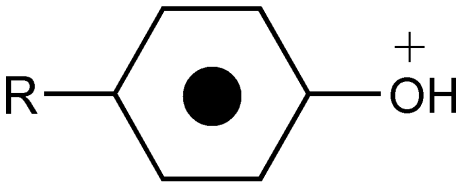

3) This convention is primarily used for visual clarity. It is also used to indicate that the radical is not solely isolated on the phenolic oxygen, but also delocalized in the ring structure.

Summary

This thesis investigates the proton-coupled electron transfer (PCET) mechanism for the reduction of the tyrosine D radical ($Y_D^{\bullet}$) in the redox-active enzyme photosystem II (PSII). I determine, through an analysis of the kinetic decay rates, that the reduction mechanism of $Y_D^{\bullet}$ is pL dependant (where pL is either p^1H or p^2H). At higher pH values (> 7.5), I use kinetic isotope effects to ascertain that $Y_D^{\bullet}$ decays by a coupled proton-electron transfer mechanism (CPET), in which both the proton and the electron are transferred in the rate determining step. At lower pL values (< 5.5), I assign the mechanism as a proton transfer-electron transfer (PTET) mechanism, where the proton is first transferred to $Y_D^{\bullet}$ in a pre-equilibrium step, followed by rate-limiting electron transfer.

Through an additional examination of my data in mixed isotopic fractions of ^1H_2O and ^2H_2O at pL 8.0, I determine that the proton transfer mechanism for $Y_D^{\bullet}$ reduction in alkaline media is more complex than previously estimated. In earlier assessments, the proton was believed to be shuttled between tyrosine D (Y_D) and an adjacent histidine, His189 of the D2 polypeptide, during the redox cycle. In this earlier mechanism, it was predicted that only the transfer of a single proton would occur. Additionally, this earlier mechanism assumed that His189 served as the only proton donor/acceptor to $Y_D^{\bullet}/Y_D$ in the redox cycle. In this thesis, I present evidence for the existence of at least one additional proton donation pathway to $Y_D^{\bullet}$. Additionally, I determine that at least one of these proton donation pathways involves the transfer of more than one proton in the rate-limiting step.

Furthermore, I utilize high-field electron paramagnetic resonance (EPR) to investigate the local environment of $Y_D^{\bullet}$ and the symmetrically analogous tyrosine Z radical, $Y_Z^{\bullet}$. Tyrosine Z (Y_Z) is tyrosine 161 in the D1 polypeptide. In those experiments, I use the fact that the g_x component of the tyrosyl radical EPR g-tensor is sensitive to the surrounding environment. Additionally, the g_x component is highly sensitive to hydrogen bonding, as this component is oriented along the phenol C-O bond. I determine that the environment of $Y_D^{\bullet}$ changes little as the pH is lowered from pH 8.0 to pH 5.0. Additionally, the data is consistent with an assignment of a hydrogen bond to a neutral His189. These results suggest that His189 is likely involved in the transfer of at least two protons during the reduction and oxidation of Y_D. An examination of $Y_Z^{\bullet}$ indicates a changing environment that becomes more electropositive as the pH is increased from 5.0 to 8.0. This is assigned to either a change in the hydrogen bond distance, the hydrogen bond orientation, or the acquisition of additional hydrogen bonding partners as the pH is increased. Additionally, the g_x components for $Y_Z^{\bullet}$ suggest a hydrogen bond to a neutral species across the pH range examined.

Taken together, this work suggests that PCET theory is useful in determining the mechanism for $Y_D^{\bullet}$ reduction. The examination of solvent kinetic isotope effects is able to determine the type of PCET mechanism occurring during $Y_D^{\bullet}$ reduction. Additionally, the use of mixed isotope fractions has allowed better understanding of the number of protons transferred in the rate-determining step of $Y_D^{\bullet}$ reduction, as well as the number of proton donation pathways involved. Finally, high-field EPR is useful for probing the protein environment surrounding $Y_D^{\bullet}$ and $Y_Z^{\bullet}$.

Chapter 1

Introduction

1.1 Photosynthesis

Photosynthesis is the most fundamental process of energy acquisition on earth, converting light energy to chemical energy.[1] It is estimated that 4 to 17 x 10^{11} tonnes of carbon are fixed each year by the photosynthetic process, leading to an estimated annual energy accumulation of between 1 x 10^{11} and 5 x 10^{14} kJ.[2-4] Additionally, photosynthesis is the primary source of oxygen in the Earth's atmosphere.[5] The process of photosynthesis utilizes a variety of protein complexes that are responsible for energy capture and transduction.[6] The primary purpose of photosynthesis is to transfer electrons and pump protons that ultimately drive the formation of adenosine triphosphate (ATP) and reduced nicotinamide adenine dinucleotide phosphate (NADPH).[6]

The photosynthetic apparatus is located in the thylakoid membrane of plants, cyanobacteria and algae.[7] In eukaryotes (plants and algae), the chloroplast houses the thylakoid membrane.[7] In prokaryotes, the thylakoid is constructed from invaginations within the cell membrane.[7] The photosynthetic pathway consists of four trans-membrane thylakoid proteins.[6,7] These proteins are photosystem II (PSII), cytochrome b_6f, photosystem I (PSI) and ATP synthase (Figure 1).[6-8] We are currently engaged in the study of the photosystem II complex.

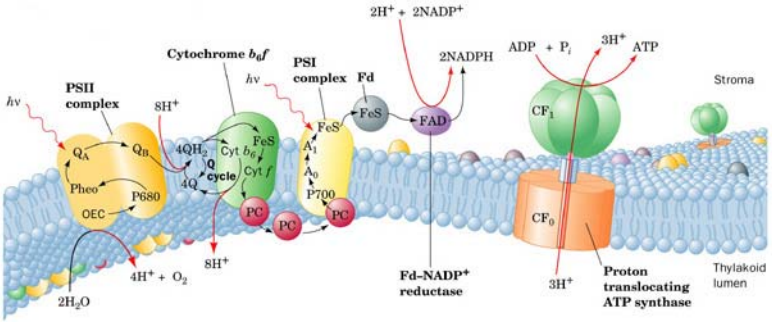

Figure 1. Illustration showing important proteins and cofactors associated with the photosynthetic apparatus.[9]

Catalysis in PSII occurs through a four photon/four electron mechanism, which is described by the Kok cycle (Figure 2).[10] PSII catalyzes two types of reactions.[11,12] The first reaction is the oxidation of two molecules of water to form one molecule of oxygen and four protons.[11,12] The second reaction is the reduction of two plastoquinone molecules to form two plastoquinol molecules.[11,12] The four electrons and four protons generated by PSII are shuttled to cytochrome b_6f by these two plastoquinols.[12,13] Cytochrome b_6f serves as an intermediary in the electron transport from PSII to PSI.[13] Additionally, cytochrome b_6f transports approximately eight to twelve protons per four electrons from the stroma to the lumen, depending on light and cellular conditions.[14] Electrons are passed from cytochrome b_6f to PSI by means of plastocyanin, a water-soluble copper-containing protein located on the luminal side of the thylakiod.[6,12,13] PSI, another light activated enzyme, reduces ferredoxin, which is in turn oxidized by ferredoxin:$NADP^+$ reductase.[12] NADPH is produced by two molecules of reduced ferredoxin:$NADP^+$ reductase, $NADP^+$ and a proton.[6] The NADPH generated then enters into the Calvin cycle.[6] ATP synthase utilizes the proton gradient generated during the

photosynthetic process to produce ATP from adenosine diphosphate (ADP) and inorganic phosphate.[6]

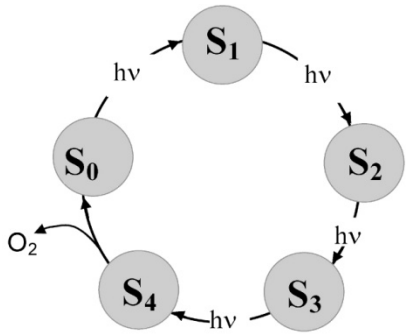

Figure 2. The Kok cycle.[15] The different oxidation states are denoted as S_n, where n is the number of oxidizing equivalents stored and S_4 is the highest oxidation state

PSII is an approximately 350 kDa trans-membrane protein (Figure 3). Crystal structures have been determined at 3.8-2.9 Å resolution.[16-19] The highest resolution crystal structure has identified 20 individual subunits in PSII.[19] Additionally, a large number of cofactors have been identified. These cofactors include 35 chlorophyll *a* molecules, 12 *β*-carotene molecules, two pheophytin *a* molecules, two plastoquinone molecules, two heme molecules, one non-heme iron atom, four manganese atoms, and one calcium atom.[19] PSII possesses both a catalytically active branch and a catalytically inactive branch.[19] The catalytically active branch consists of cofactors that primarily reside in the D1 polypeptide, whereas the catalytically inactive branch consists of cofactors that primarily reside on the D2 polypeptide.[19] The catalytic mechanism is initiated by the absorption of visible light, resulting in charge separation between the primary donor Chl and $Pheo_{D1}$, a pheophytin *a* molecule in the D1 subunit.[20,21] Controversy exists over the identity of the electron donor to $Pheo_{D1}$.[20-22] Primary charge

separation is believed to occur between Chl_{D1} and $Pheo_{D1}$ and the positive hole left after Chl_{D1} electron transfer is thought to be transferred to P_{680}.[23] P_{680} is a chlorophyll dimer consisting of P_{D1} and P_{D2} of the D1 and D2 subunit, respectively.[20,23] P_{680}^{+} oxidizes a tyrosine, Y_Z (Tyr161 on the D1 subunit). The reduction of P_{680}^{+} occurs on the order of nanoseconds in oxygen evolving PSII.[24,25] However, when PSII is depleted of the oxygen evolving complex (OEC), the timescale is slowed to microseconds.[26,27] The OEC is a $Ca[Mn]_4$ metallocluster on the D1 polypeptide where water oxidation occurs.[28] $Y_Z^{\bullet}$ is responsible for the oxidation of the OEC.[29] The oxidation of the OEC occurs on the microseconds to milliseconds timescale, depending on the number of oxidizing equivalents stored.[30,31] The OEC stores four oxidizing equivalents before converting two molecules of water into molecular oxygen and four protons.[32] The different oxidation states of the OEC are denoted as S_n, where n is the number of oxidizing equivalents stored and S_4 is the highest oxidation state (Figure 2).[11] $Pheo_{D1}$ reduces a plastoquinone single-electron acceptor, Q_A, on the picoseconds timescale.[33,34] Q_A^{-} then reduces the plastoquinone terminal electron acceptor, Q_B, in the microseconds timescale.[35,36] Q_B resides on the D2 polypeptide and is the only catalytically active cofactor that does not reside on the D1 polypeptide.[16-19] Q_B exits PSII and enters into the quinone pool as a quinol (Q_BH_2) upon two electron reduction and the acquisition of two protons.[28] The doubly reduced quinol is then replaced by a fully oxidized quinone, completing the catalytic cycle.[28] The quinone is believed to be replaced by a diffusion process; however, other mechanisms have recently been proposed.[17]

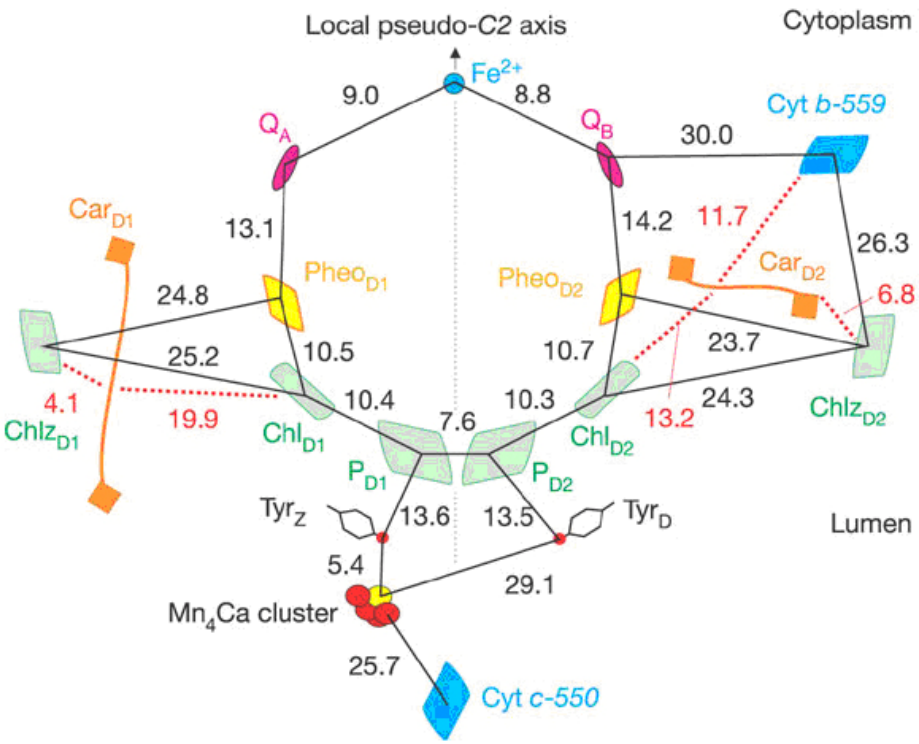

Figure 3. Diagram showing the PSII cofactors and their relative orientation.[19] The dotted horizontal line roughly divides the D1 (left) and D2 (right) polypeptides. The solid black lines represent distances in Å.

The catalytically inactive D2 polypeptide possesses all of the cofactors of the catalytically active D1 polypeptide, with the important exception of the OEC.[28] In the D2 polypeptide there is a tyrosine, Y_D (Tyr160 on the D2 subunit), that is analogous to Y_Z. Y_D and Y_Z are both approximately 13-14 Å from P_{680}.[16-19] Each tyrosine also has a histidine within hydrogen bonding distance, His189 on the D2 polypeptide in the case of Y_D (Scheme 1) and His190 on the D1 polypeptide in the case of Y_Z.[19] Despite their structural similarity, there are significant differences between these two tyrosines. First, their midpoint potentials differ by about 240 mV, with $Y_Z^{\bullet}/Y_Z$ (~930 mV) having a higher midpoint potential than $Y_D^{\bullet}/Y_D$ (~690 mV).[37-40] Additionally, Y_D is hydrogen bonded,[41-46] whereas Y_Z is either in a highly disordered environment or is not hydrogen

bonded.[44,45,47-50] Furthermore, while both tyrosine radicals have similar spectroscopic characteristics, the decay kinetics between the two are vastly different.[30,32,51] $Y_D^{\bullet}$ decays on the minutes to hours time scale, whereas $Y_Z^{\bullet}$ decays on the microseconds to milliseconds time scale.[52]

Scheme 1

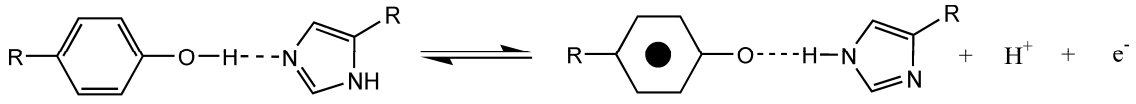

The study of $Y_D^{\bullet}$ is facilitated by its long decay time.[51] $Y_D^{\bullet}$ has been proposed to be involved in the dark stabilization of the OEC by accepting an electron from the OEC when it is in the S_0 state, placing the OEC in the more stable S_1 oxidation state.[51] Additionally, Y_D is able to donate an electron to the OEC in the higher energy S_2 state and reduce it to the more stable S_1 resting state.[51] In bacterial systems, where phenylalanine has been substituted for Y_D, photosynthetic growth is still observed; however, the organism grows more slowly.[53] The implication is that Y_D, while not essential for photosynthetic activity, is important in influencing the efficiency of PSII, potentially acting in a redox role or altering the electrostatics of PSII.[51]

$Y_D^{\bullet}$, the electron acceptor in the studies presented herein, has been unambiguously identified through site-directed mutagenesis[53] and global isotopic labeling.[54] However the identity of the electron donor is not as clear, as PSII contains multiple redox active cofactors (Figure 3). Fortunately, there are few reductants to $Y_D^{\bullet}$ in PSII that have half-lives as long as $Y_D^{\bullet}$ itself. One reducing species that does have a

half-life on the order observed in these studies is Q_A^-. Johnson et al.[55] and Demeter et al.[56] independently determined, using thermoluminescence and EPR data, that Q_A^- acts as a donor to $Y_D^{\bullet}$.

1.2 Electron Paramagnetic Resonance (EPR) Spectroscopy

Electron paramagnetic resonance spectroscopy, also known as electron spin resonance spectroscopy, is a form of microwave spectroscopy that is unambiguously able to detect unpaired electrons.[57-59] Since an electron has two spin quantum numbers, where m_s is either ½ or -½, the spin can be aligned parallel or anti-parallel to an applied magnetic field.[57,58] The result is an electron having two different available energy levels.[57,58] When Equation 1 is satisfied, resonance is achieved between the two energy levels.

$$h\nu = g_e \mu_B B_0$$

Equation 1. The equation for EPR resonance.[57-59]

In Equation 1, h is Planck's constant, ν is the frequency (usually in GHz), g_e is the electron g-factor, μ_B is the Bohr magneton and B_0 is the magnetic field strength.[57-59] Figure 4 depicts schematically the resonance that occurs when Equation 1 is satisfied. As indicated in Figure 4, population of the lower energy state is almost always higher than that of the higher energy state, due to the Maxwell-Boltzmann distribution.[57,58] As a result, there is a net absorption of energy under resonance conditions.[57,58]

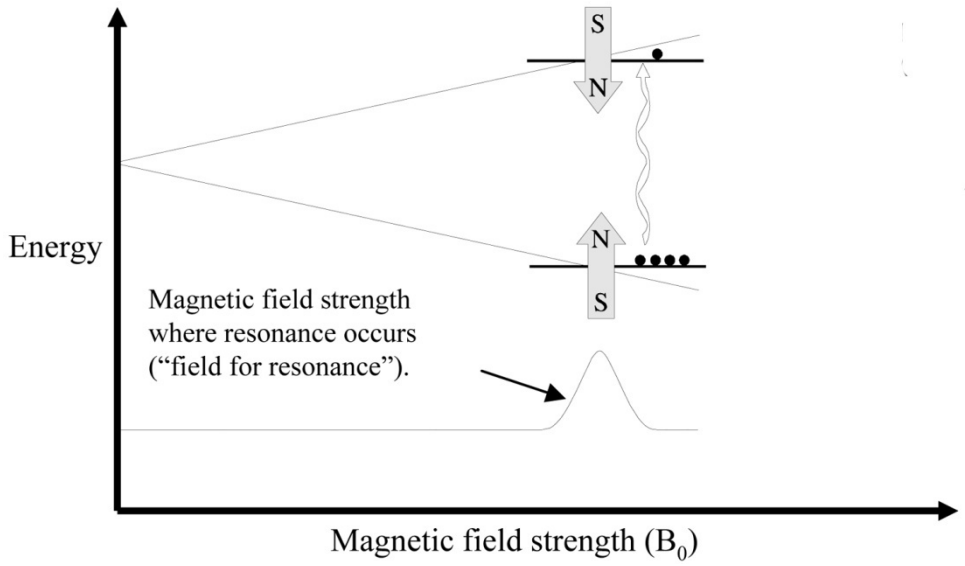

Figure 4. Resonance in an EPR spectrometer.[59]

In EPR spectroscopy, either the frequency or the magnetic field can be varied in theory, but usually it is only the magnetic field that is altered.[57-59] This occurs for various reasons. Most importantly, many microwave frequency generators have only a range of between 5-10% of their center frequency.[57,58] Additionally, the tuning of the microwave transmission line is frequency sensitive, and scanning the frequency would require constant tuning of multiple components.[57] Finally, power output for certain microwave frequency generators varies by frequency, so a power stabilizer would be required.[57] The above limitations are eliminated when the magnetic field is scanned.[57,59]

EPR spectroscopy is useful, not only because it can give information about free electron itself, but also because it relays information about the surrounding environment.[57-59] This occurs because unpaired electron spin is often delocalized about the area where it is centrally located.[57,58] When an electron interacts with a nucleus of appropriate spin, the electron under interrogation acquires additional, smaller energy

levels.[57,58] This occurs because the electron is able to interact in a manner parallel or anti-parallel to the nuclear spin.[57,58] This process is analogous to that observed in proton splitting in ^{1}H-NMR spectroscopy.[57,58] The resulting splitting pattern is known as hyperfine coupling (Figure 5).[57-59] The electron's signal is split by M equivalent nuclei according to Equation 2; where hfc is the number of hyperfine couplings observed, M is the number of equivalent nuclei and I is the nuclear spin quantum number for those nuclei.[57,58]

$$\text{hfc} = 2\text{MI} + 1$$

Equation 2. Hyperfine coupling for M equivalent nuclei.

For a system with more than one equivalent nuclei, the general form of the equation can be used (Equation 3); where hfc is the resulting number of hyperfine couplings, M_i is the number of *i*th equivalent nuclei and I_i is the nuclear spin quantum number for the *i*th equivalent nuclei.[57,58]

$$\text{hfc} = \prod_i (2\text{M}_i\text{I}_i + 1)$$

Equation 3. The general form of the equation for hyperfine coupling, used when more than one type of nuclei are present.

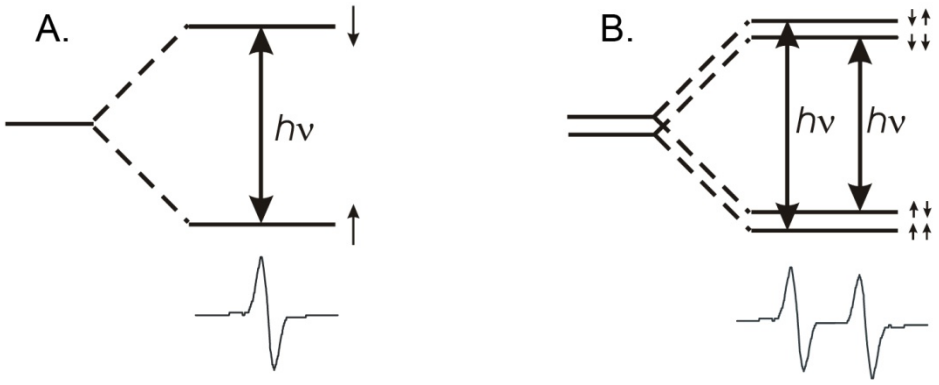

Figure 5. A. Sample having no hyperfine coupling and B. Splitting of an EPR signal by a nearby nucleus with I = ½.[59]

There are various microwave frequencies available for EPR spectroscopy.[57] The most popular frequency is between nine and ten GHz, known as X-band.[57] The popularity of X-band EPR is largely due to two factors. EPR development began after World War II, when X-band microwave generators were widely used for radar systems. This resulted in an abundant surplus of X-band microwave generators.[57] Secondly, X-band spectrometers require magnetic fields of approximately 3500 G.[58,59] Stable magnetic fields of this magnitude are easily obtained in electromagnets.[57] Other magnetic frequencies commonly used in EPR spectroscopy are listed in Table 1.

Table 1. Common microwave bands used in EPR and the corresponding magnetic field for the resonance of a free electron (g_e = 2.002319).[60]

Band	**Frequency Range (GHz)**	**Magnetic Field Range (G)**
L	1-2	357-714
S	2-4	714-1427
X	8-12	2,855-4,282
Q	30-50	10,705-17,841
W	75-110	26,762-39,251
D	110-170	39,251-60,660

Electromagnetic waves have both a magnetic and electronic component.[59] In EPR spectroscopy, it is the magnetic component that drives the absorption.[59] Since water is a highly lossy matrix in the microwave region (i.e. it absorbs the electronic component of the electromagnetic wave), the analysis of biological samples requires special techniques in order to be able to observe magnetic resonance.[57-59] Since it is only the electronic component of the electromagnetic wave which is absorbed by water, specialized cells are utilized that are able to minimize the absorption of the electronic component in the sample cavity.[57,59] In Figure 6, it can be observed that the magnetic and electronic components are out of phase with one another in an EPR resonator.[57,59] This allows the sample to be placed simultaneously in a magnetic field maximum and an electronic field minimum.[59] The placement of the sample in the optimum orientation is achieved by the use of a flat cell or a capillary, which conveniently fits in the valley of the electromagnetic component.[57,59] The result is the ability to analyze aqueous samples that would otherwise be impossible.

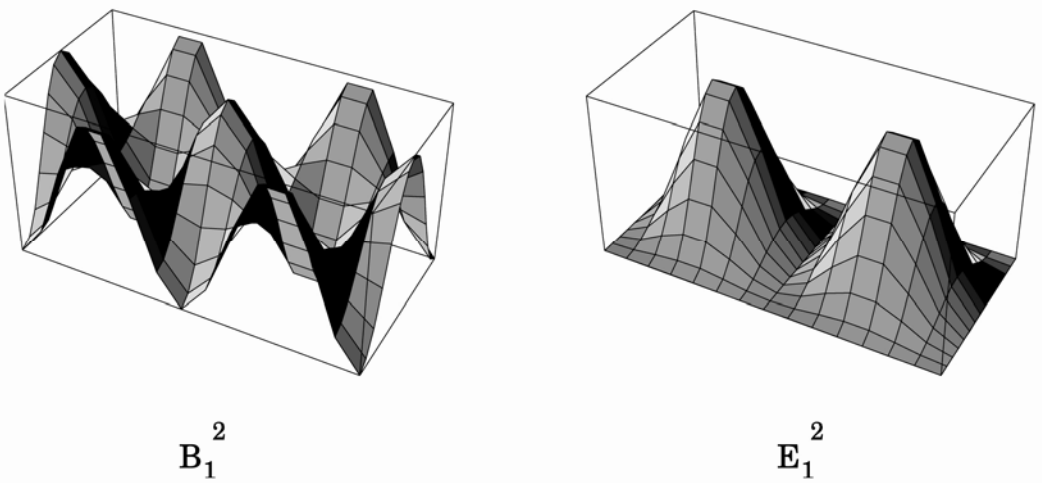

Figure 6. Field density in a typical (TE_{102}) EPR resonator. B_1^2 is the square of the magnetic field intensity. E_1^2 is the square of the electronic field intensity.[59]

1.3 Infrared Spectroscopy

Infrared spectroscopy is an analytical technique that measures the vibrational transitions in a molecule.[61] These vibrational transitions provide information about the chemical bond.[61] The vibrational frequency for a chemical bond is related to the reduced mass and the force constant in the harmonic oscillator equation (Equation 4), where *v* is the frequency, k is the bond strength, and μ is the reduced mass.[61]

$$v = \frac{1}{2\pi}\sqrt{\frac{k}{\mu}}$$

Equation 4. The harmonic oscillator equation.[61]

The reduced mass is given by Equation 5, where μ is the reduced mass, m_A and m_B are the masses of atom A and atom B in the chemical bond, respectively.[61]

$$\mu = \frac{m_A * m_B}{m_A + m_B}$$

Equation 5. The reduced mass equation.[61]

Infrared measurements can typically be made through one of two ways. The first is through dispersive techniques where the infrared beam is separated into its component wavelengths by a grating or prism and the vibrational frequency is measured one wavelength at a time.[62] However, most current infrared spectrometers now use Fourier transform (FT) techniques.[62] In Fourier transform infrared (FT-IR) spectroscopy (Figure 7), an interferometer is employed to capture data in the time domain. An interferometer consists of fixed mirror, a moving mirror and a beamsplitter.[62] As the moving mirror oscillates, constructive and destructive interferences are created upon recombination of the reflected beams from the stationary and moving mirrors. These constructive and

destructive interferences will change over time as the moving mirror changes position, resulting in an interferogram. The subsequent use of a Fourier transform converts the acquired data from the time domain to the frequency domain.

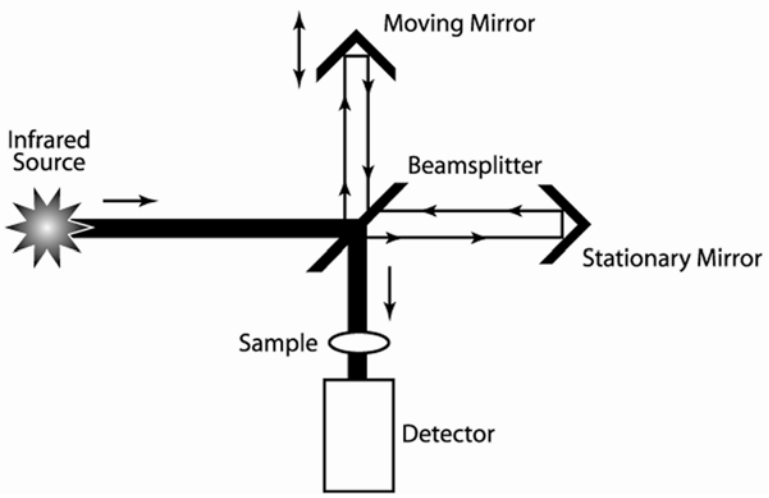

Figure 7. Basic diagram of an FT-IR spectrometer employing an interferometer.[62]

The FT-IR spectrometer has a number of advantages over the dispersive type.[62] First, the multiplex advantage allows more rapid collection of data.[62] This is because FT-IR instruments scan every wavelength simultaneously, whereas dispersive instruments scan only one wavelength at a time.[62] This results in FT-IR instruments acquiring more scans in a given unit of time.[62] The second benefit is Fellgett's advantage, also known as throughput advantage.[62] Fellgett's advantage results from the fact that there are fewer mirror sources in an FT-IR spectrometer, resulting in less dispersive losses.[62] The result is a higher energy throughput to the detector and an improved signal-to-noise ratio.[62] The final improvement that FT-IR has over dispersive IR is higher precision.[62] Since FT-IR

spectrometers utilize a laser to control the moving mirror, an internal wavelength calibration may simultaneously be employed.[62]

A technique useful in FT-IR spectroscopy for evaluating biological samples is attenuated total reflectance (ATR). ATR/FT-IR spectroscopy is able to improve the acquisition of the infrared spectrum in the presence of water.[63,64] In acquiring an ATR/FT-IR spectrum, the ATR unit is placed in the IR beam pathway.[63,64] The beam is then internally reflected through a crystal, upon which the sample is in contact (Figure 8).[63,64] This process creates an evanescent wave that slightly extends into the sample medium. The depth of penetration is frequency dependant, but typically is between 0.5-5 micrometers.[64] As the sample absorbs IR radiation, the signal size is decreased, or attenuated.[63,64] The resulting spectrum is similar to a transmission spectrum, but there are differences.[63] The primary difference is due to the wavelength dependant penetration of the evanescent wave.[63] This results in a lower relative intensity in the higher wavenumber region.[63] The second difference is that the spectrum contains not only the absorption, but also the reflectance characteristics of the sample under interrogation.[63] One useful property of ATR/FT-IR spectroscopy is the ability to subtract the spectrum of the solvent or buffer, allowing better resolution for the sample under study.

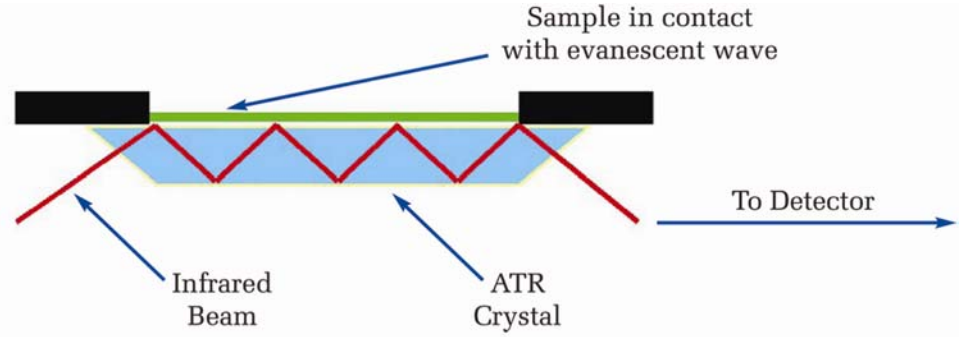

Figure 8. Attenuation of the IR beam through an ATR cell. Displayed is a crystal that has four internal reflections.[64]

Enzyme function and structure are commonly studied by FT-IR spectroscopy.[65] The primary modes of the amide backbone are known and assigned in the infrared spectrum.[65] The two most commonly used primary modes used to establish secondary structure information in proteins are known as Amide I and Amide II.[65,66] The Amide I band is observed in the 1620-1700 cm^{-1} region.[65,66] Amide I primarily represents vibrations arising from C=O stretching (~80%) and an out-of-phase CN stretch (~15%).[65] The Amide II band is normally observed in the 1510-1580 cm^{-1} region.[65] It consists primarily of NH in-plane bending (~50%), and CN stretching (~35%).[65] Isotopic substitution, site-directed mutagenesis and light-induced changes have been utilized in the study of the structure and mechanism of enzymes in conjunction with FT-IR spectroscopy.[67-71]

1.4 Proton-Coupled Electron Transfer

Proton-coupled electron transfer (PCET) is an electrochemical process that involves the transfer of both an electron and a proton.[72-76] The transfer of the proton and electron can occur in either a stepwise or concerted pathway.[72-76] Furthermore, in the

stepwise mechanism, either the proton or electron may be transferred first.[72-76] When the proton is transferred first, the process is known as the PTET (proton transfer followed by electron transfer) mechanism. When the electron is transferred first the mechanism is known as the ETPT (electron transfer followed by proton transfer) mechanism. Finally, when the electron and proton are transferred in a single kinetic step, the mechanism is known as the CPET (coupled proton-electron transfer) mechanism. If the proton is transferred in the rate-limiting step, kinetic isotope effects (KIE) are often observed.[77-81] KIEs can be diagnostic of PCET reaction mechanisms.[77-81]

PCET reactions depend on both the redox potential, E, and the pK_a The redox potential is important for determining the rate of electron transfer, while the pK_a influences the rate of the proton transfer.[76] However, both are still free energy processes.[76] Bordwell has demonstrated that bond strength can be calculated by experimentally determining pK_a and E.[82] If these two variables are known, a square scheme (Scheme 2) can be used to calculate the bond strength.[76] This is possible because all three pathways must have equal energies.[76] Therefore, setting the two one-step pathways equal, the energy of the diagonal step can be determined.[76] Equation 6 can be used for this calculation, where n is the number of electrons being transferred, F is the Faraday constant, R is the gas constant and T is the temperature in Kelvin.[76]

$$2.3\mathrm{RT} * \mathrm{p}K_a(\mathrm{XH}^{\bullet+}) + \mathrm{nF} * E(\mathrm{HX}^{\bullet+}/\mathrm{HX}) = 2.3\,\mathrm{RT} * \mathrm{p}K_a(\mathrm{XH}) + 2.3\mathrm{nF} * E(\mathrm{X}^{\bullet}/\mathrm{X}^{-})$$

Equation 6. Equality of energy between both two step processes in Scheme 2.[76]

It can be seen from the above equation that a change in the redox potential will have an opposite and equal effect on the pK_a, providing that the bond strength remains constant.[76] This result is important in PCET, because the generation of a radical (or the

reduction of the radical) can cause profound changes in the pK_a. A common example in biochemistry is tyrosine. Neutral tyrosine has a pK_a of 10. Upon formation of the tyrosyl radical, the pK_a becomes much more acidic (pK_a = -2), a change in acidity of approximately twelve orders of magnitude. In photosystem II, Y_D donates a proton to His189 upon radical generation, preventing the formation of the high energy tyrosyl cation intermediate.

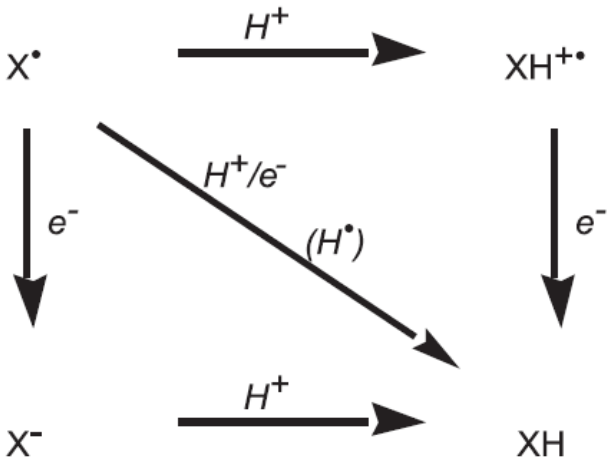

Scheme 2. Square scheme for the reduction and protonation of a radical.[76]

A technique that is useful for the determination of the reaction mechanism when a proton is transferred in the rate-limiting step is the proton inventory experiment.[83-85] In the proton inventory experiment, mixed solutions of ^1H_2O:^2H_2O are employed.[83-85] When the mole fraction ^2H_2O is plotted against the rate, conclusions can be drawn about the number of protons transferred in the rate-limiting step.[83-85] A linear plot generally indicates a single proton being transferred in the rate-limiting step.[83-86] A quadratic plot indicates two proton transfer in the rate-limiting step.[83-85,87] A logarithmic plot indicates

that three of more protons are being transferred in the rate-limiting step.[83-85,88] It can also occasionally occur that a plot is bowed downward more deeply than the logarithmic plot.[83-85] Plots of this type are said to exhibit hypercurvature.[83-85] Plots displaying hypercurvature generally have more complex interpretations than plots exhibiting linear, quadratic and exponential behavior.[83-85]

1.4 Scope of Thesis

This thesis will examine the mechanism of $Y_D^{\bullet}$ decay. The decay rate of $Y_D^{\bullet}$ as a function of pL (where L is either ^1H or ^2H) will be examined in pure ^1H_2O, pure ^2H_2O, and mixed proportions of ^1H_2O:^2H_2O to determine mechanism of radical decay. Additionally, we will use high-field EPR analysis to determine the protonation state of $Y_D^{\bullet}$ and $Y_Z^{\bullet}$ across a range of pH values.

1.5 References

(1) Arnon, D. I. Conversion of light into chemical energy in photosynthesis. *Nature* **1959**, *184*, 10-21.

(2) Rabinowitch, E.; Govindjee *Photosynthesis*; Wiley: New York, 1969.

(3) Field, C. B.; Behrenfeld, M. J.; Randerson, J. T.; Falkowski, P. Primary production of the biosphere: Integrating terrestrial and oceanic components. *Science* **1998**, *281*, 237-240.

(4) Nealson, K. H.; Conrad, P. G. Life: past, present and future. *Philos. Trans. R. Soc. London, Ser. B* **1999**, *354*, 1923-1939.

(5) Falkowski, P. G.; Godfrey, L. V. Electrons, life and the evolution of Earth's oxygen cycle. *Philosophical Transactions of the Royal Society B-Biological Sciences* **2008**, *363*, 2705-2716.

(6) Voet, D.; Voet, J. G. *Biochemistry*; J. Wiley & Sons: New York, 1995.

(7) Vermaas, W. Revealing the secrets of old sol's sugar factories. *The World & I* **1998**, *13*, 8.

(8) Whitmarsh, J. G. *Concepts in Photobiology: Photosynthesis and Photomorphogenesis*; Kluwer Academic Press: Boston, 1999.

(9) Voet, D. J.; Voet, J. G. *Biochemistry*; 3rd ed.; J. Wiley & Sons: New York, 2004.

(10) Kok, B.; Forbush, B.; McGloin, M. Cooperation of charges in photosynthetic O_2 evolution-1. A linear four step mechanism. *Photochem. Photobiol.* **1970**, *11*, 457-471.

(11) Babcock, G. T.; Barry, B. A.; Debus, R. J.; Hoganson, C. W.; Atamian, M.; McIntosh, L.; Sithole, I.; Yocum, C. F. Water oxidation in photosystem II: From radical chemistry to multielectron chemistry. *Biochemistry* **1989**, *28*, 9557-9565.

(12) Nelson, N.; Yocum, C. F. Structure and function of photosystems I and II. *Annu. Rev. Plant Biol.* **2006**, *57*, 521-565.

(13) Baniulis, D.; Yamashita, E.; Zhang, H.; Hasan, S. S.; Cramer, W. A. Structure-function of the cytochrome b_6f complex. *Photochem. Photobiol.* **2008**, *84*, 1349-1358.

(14) Shikanai, T.; Munekage, Y.; Kimura, K. Regulation of proton-to-electron stoichiometry in photosynthetic electron transport: Physiological function in photoprotection. *J. Plant Res.* **2002**, *115*, 3-10.

(15) Shinkarev, V. P. Oxygen evolution in photosynthesis: Simple analytical solution for the Kok model. *Biophys. J.* **2003**, *85*, 435-441.

(16) Zouni, A.; Witt, H.-T.; Kern, J.; Fromme, P.; Krauß, N.; Saenger, W.; Orth, P. Crystal structure of photosystem II from *Synechococcus elongatus* at 3.8 Å resolution. *Nature* **2001**, *409*, 739-743.

(17) Guskov, A.; Kern, J.; Gabdulkhakov, A.; Broser, M.; Zouni, A.; Saenger, W. Cyanobacterial photosystem II at 2.9- Å resolution and the role of quinones, lipids, channels and chloride. *Nat. Struct. Mol. Biol.* **2009**, *16*, 334-342.

(18) Ferreira, K. N.; Iverson, T. M.; Maghlaoui, K.; Barber, J.; Iwata, S. Architecture of the photosynthetic oxygen-evolving center. *Science* **2004**, *303*, 1831-1837.

(19) Loll, B.; Kern, J.; Saenger, W.; Zouni, A.; Biesiadka, J. Towards complete cofactor arrangement in the 3.0 Å resolution structure of photosystem II. *Nature* **2005**, *438*, 1040-1044.

(20) Diner, B. A.; Rappaport, F. Structure, dynamics, and energetics of the primary photochemistry of photosystem II of oxygenic photosynthesis. *Annu. Rev. Plant Biol.* **2002**, *53*, 551-580.

(21) Holzwarth, A. R.; Muller, M. G.; Reus, M.; Nowaczyk, M.; Sander, J.; Rogner, M. Kinetics and mechanism of electron transfer in intact photosystem II and in the isolated reaction center: Pheophytin is the primary electron acceptor. *Proc. Natl. Acad. Sci. USA* **2006**, *103*, 6895-6900.

(22) Groot, M. L.; Pawlowicz, N. P.; van Wilderen, L.; Breton, J.; van Stokkum, I. H. M.; van Grondelle, R. Initial electron donor and acceptor in isolated Photosystem II reaction centers identified with femtosecond mid-IR spectroscopy. *Proc. Natl. Acad. Sci. USA* **2005**, *102*, 13087-13092.

(23) Diner, B. A.; Schlodder, E.; Nixon, P. J.; Coleman, W. J.; Rappaport, F.; Lavergne, J.; Vermaas, W. F. J.; Chisholm, D. A. Site-directed mutations at D1-His198 and D2-His197 of photosystem II in *Synechocystis* PCC 6803: sites of primary charge separation and cation and triplet stabilization. *Biochemistry* **2001**, *40*, 9265-9281.

(24) Gerken, S.; Brettel, K.; Schlodder, E.; Witt, H. T. Optical characterization of the immediate donor to Chlorophyll a_{II}^{+} in O_2-evolving photosystem II complexes. *FEBS Lett.* **1988**, *237*, 69-75.

(25) Schlodder, E.; Meyer, B. pH dependence of oxygen evolution and reduction kinetics of photooxidized chlorophyll a_{II} (P_{680}) in Photosystem II particles from *Synechococcus* sp. *Biochim. Biophys. Acta* **1987**, *890*, 23-31.

(26) Boska, M.; Sauer, K.; Buttner, W.; Babcock, G. T. Similarity of EPR Signal II_f rise and P_{680}^+ decay kinetics in Tris-washed chloroplast photosystem II preparations as a function of pH. *Biochim. Biophys. Acta* **1983**, *722*, 327-330.

(27) Conjeaud, H.; Mathis, P. The effect of pH on the reduction kinetics of P_{680} in Tris-treated chloroplasts. *Biochim. Biophys. Acta* **1980**, *590*, 353-359.

(28) Whitmarsh, J. G. In *Encyclopedia of Life Sciences*; John Wiley and Sons, Ltd.: Chichester, 2002.

(29) Boerner, R. J.; Barry, B. A. Isotopic labeling and EPR spectroscopy show that a tyrosine residue is the terminal electron donor, Z, in manganese-depleted photosystem II preparations. *J. Biol. Chem.* **1993**, *268*, 17151-17154.

(30) Babcock, G. T.; Sauer, K. The rapid component of electron paramagnetic resonance Signal II: A candidate for the physiological donor to photosystem II in spinach chloroplasts. *Biochim. Biophys. Acta* **1975**, *376*, 329-344.

(31) Dekker, J. P.; Plijter, J. J.; Ouwehand, L.; Gorkom, H. J. V. Kinetics of manganese redox transitions in the oxygen-evolving apparatus of photosynthesis. *Biochim. Biophys. Acta* **1984**, *767*, 176-179.

(32) Babcock, G. T.; Sauer, K. Electron paramagnetic resonance Signal II in spinach chloroplasts. *Biochim. Biophys. Acta* **1973**, *325*, 483-503.

(33) Nuijs, A. M.; Vangorkom, H. J.; Plijter, J. J.; Duysens, L. N. M. Primary-charge separation and excitation of chlorophyll *a* in photosystem II particles from spinach as studied by picosecond absorbency-difference spectroscopy. *Biochim. Biophys. Acta* **1986**, *848*, 167-175.

(34) Trissl, H. W.; Leibl, W. Primary charge separation is photosystem II involves two electrogenic steps. *FEBS Lett.* **1989**, *244*, 85-88.

(35) Britt, R. D. In *Oxygenic Photosynthesis: The Light Reactions*; Ort, D. R., Yocum, C. F., Eds.; Kluwer Academic Publisher: Dordrecht, 1996; Vol. 4, p 137-164.

(36) Wijn, R. d.; Gorkom, H. J. v. Kinetics of electron transfer from Q_A to Q_B in photosystem II. *Biochemistry* **2001**, *40*, 11912-11922.

(37) Boussac, A.; Etienne, A. L. Midpoint potential of signal II (slow) in tris-washed photosyste II particles. *Biochim. Biophys. Acta* **1984**, *766*, 576-581.

(38) Metz, J. G.; Nixon, P. J.; Rögner, M.; Brudvig, G. W.; Diner, B. A. Directed alteration of the D1 polypeptide of photosystem II: evidence that tyrosine-161 is the redox component, Z, connecting the oxygen-evolving complex to the primary electron donor, P680. *Biochemistry* **1989**, *28*, 6960-6969.

(39) Vass, I.; Styring, S. pH-Dependent charge equilibria between Tyrosine-D and the S states in photosystem II. Estimation of relative midpoint redox potentials. *Biochemistry* **1991**, *30*, 830-839.

(40) Ishikita, H.; Knapp, E. W. Function of redox-active tyrosine in photosystem II. *Biophys. J.* **2006**, *90*, 3886-3896.

(41) Rodriguez, I. D.; Chandrashekar, T. K.; Babcock, G. T. In *Progress in Photosynthesis Research*; Biggins, J., Ed.; Martinus Nijhoff Publishers: Dordrecht, 1987; Vol. I, p 471-473.

(42) Evelo, R. G.; Dikanov, S. A.; Hoff, A. J. Electron spin-echo envelope modulation (ESEEM) studies of the tyrosyl radical D of plant photosystem II. *Chem. Phys. Lett.* **1989**, *157*, 25-30.

(43) Evelo, R. G.; Hoff, A. J.; Dikanov, S. A.; Tyryshkin, A. M. An ESEEM study of the oxidized electron donor of plant photosystem II: evidence that D is a neutral tyrosine radical. *Chem. Phys. Lett.* **1989**, *161*, 479-484.

(44) Force, D. A.; Randall, D. W.; Britt, R. D.; Tang, X.-S.; Diner, B. A. ^{2}H ESE-ENDOR study of hydrogen bonding to the tyrosine radicals $Y_D^{\bullet}$ and $Y_Z^{\bullet}$ of photosystem II. *J. Am. Chem. Soc.* **1995**, *117*, 12643-12644.

(45) Un, S.; Atta, M.; Fontecave, M.; Rutherford, A. W. g-Values as a probe of the local protein environment: High-field EPR of tyrosyl radicals in ribonucleotide reductase and photosystem II *J. Am. Chem. Soc.* **1995**, *117*, 10713-10719.

(46) Un, S.; Tang, X.-S.; Diner, B. A. 245 GHz High-field EPR study of tyrosine-$D^{\bullet}$ and Tyrosine-$Z^{\bullet}$ in mutants of photosystem II. *Biochemistry* **1996**, *35*, 679-684.

(47) Bernard, M. T.; MacDonald, G. M.; Nguyen, A. P.; Debus, R. J.; Barry, B. A. A difference infrared study of hydrogen bonding to the Z tyrosyl radical of photosystem II. *J. Biol. Chem.* **1995**, *270*, 1589-1594.

(48) Tommos, C.; Tang, X.-S.; Warncke, K.; Hoganson, C. W.; Styring, S.; McCracken, J.; Diner, B. A.; Babcock, G. T. Spin-density distribution, conformation, and Hydrogen bonding of the redox-active tyrosine Y_z in photosystem II from multiple electron magnetic resonance spectroscopies: Implications for photosynthetic oxygen evolution. *J. Am. Chem. Soc.* **1995**, *117*, 10325-10335.

(49) Tang, X. S.; Zheng, M.; Chisholm, D. A.; Dismukes, G. C.; Diner, B. A. Investigation of the differences in the local protein environments surrounding tyrosine radicals $Y_Z^{\bullet}$ and $Y_D^{\bullet}$ in photosystem II using wild-type and the D2-Tyr160Phe mutant of *Synechocystis* 6803. *Biochemistry* **1996**, *35*, 1475-1484.

(50) Diner, B. A.; Force, D. A.; Randall, D. W.; Britt, R. D. Hydrogen bonding, solvent exchange, and coupled proton and electron transfer in the oxidation and reduction of redox-active tyrosine Y_Z in Mn-depleted core complexes of photosystem II. *Biochemistry* **1998**, *37*, 17931-17943.

(51) Rutherford, A. W.; Boussac, A.; Faller, P. The stable tyrosyl radical in Photosystem II: why D? *Biochim. Biophys. Acta* **2004**, *1655*, 222-230.

(52) Ma, C.; Barry, B. A. Electron paramagnetic resonance characterization of tyrosine radical, M^+, in site-directed mutants of photosystem II. *Biophys. J.* **1996**, *71*, 1961-1972.

(53) Debus, R. J.; Barry, B. A.; Babcock, G. T.; McIntosh, L. Site-specific mutagenesis identifies a tyrosine radical involved in the photosynthetic oxygen-evolving complex. *Proc. Natl. Acad. Sci. USA* **1988**, *85*, 427-430.

(54) Barry, B. A.; Babcock, G. T. Tyrosine radicals are involved in the photosynthetic oxygen-evolving system. *Proc. Natl. Acad. Sci. USA* **1987**, *84*, 7099-7103.

(55) Johnson, G. N.; Boussac, A.; Rutherford, A. W. The origin of 40-50 $^{\circ}$C thermoluminescence bands in photosystem II. *Biochim. Biophys. Acta* **1994**, *1184*, 85-92.

(56) Demeter, S.; Goussias, C.; Bernat, G.; Kovacs, L.; Petrouleas, V. Participation of the g = 1.9 and g = 1.82 EPR forms of the semiquinome-iron complex Q_A^-/Fe^{2+} of photosystem II in the generation of the Q and C thermoluminescence bands, respectively. *FEBS Lett.* **1993**, *336*, 352-356.

(57) Poole, C. P. *Electron Spin Resonance: A Comprehensive Treatise on Experimental Techniques*; Dover Publications: Mineola, N.Y., 1996.

(58) Weil, J. A.; Bolton, J. R. *Electron Paramagnetic Resonance: Elementary Theory and Practical Applications*; Wiley: New York, 1994.

(59) Bruker Biospin *Bruker BioSpin EPR User Service Training Course*; Bruker BioSpin: Billerica, MA, 2003.

(60) Dikanov, S. A.; Crofts, A. R. In *Handbook of Applied Solid State Spectroscopy*; Vij, D. R., Ed.; Springer: New York, 2006, p 97-149.

(61) McQuarrie, D. A.; Simon, J. D. *Physical Chemistry: A Molecular Approach*; University Science Books: Sausalito, Calif., 1997.

(62) ThermoNicolet *FT-IR vs. Dispersive Infrared: Theory of Infrared Spectroscopy Instrumentation*, 2002.

(63) Grdadolnik, J. ATR-FTIR spectroscopy: Its advantages and limitations. *Acta Chimica Slovenica* **2002**, *49*, 631-642.

(64) Perkin Elmer *FT-IR Spectroscopy Attenuated Total Reflectance (ATR)*, Perkin Elmer, 2005.

(65) Krimm, S.; Bandekar, J. In *Adv. Protein Chem.*; Anfinsen, C. B., Edsall, J. T., Richards, F. M., Eds.; Academic Press: New York, 1986; Vol. 38, p 181-364.

(66) Grdadolnik, J. Saturation effects in FTIR spectroscopy: Intensity of Amide I and Amide II bands in protein spectra. *Acta Chimica Slovenica* **2003**, *50*, 777-788.

(67) Kim, S.; Barry, B. A. Reaction induced FT-IR spectroscopic studies of biological energy conversion in oxygenic photosynthesis and transport. *J. Phys. Chem. B* **2001**, *105*, 4072-4083.

(68) Bender, S. L.; Barry, B. A. Light-induced dynamics in photosystem I electron transfer. *Biophys. J.* **2008**, *95*, 3927-3934.

(69) Bender, S. L.; Keough, J. M.; Boesch, S. E.; Wheeler, R. A.; Barry, B. A. The vibrational spectrum of the secondary electron acceptor, A_1, in photosystem I. *J. Phys. Chem. B* **2008**, *112*, 3844-3852.

(70) Kim, S.; Liang, J.; Barry, B. A. Chemical complementation identifies a proton acceptor for redox-active tyrosine D in photosystem II. *Proc. Natl. Acad. Sci. USA* **1997**, *94*, 14406-14412.

(71) Friedrich, T.; Geibel, S.; Kalmbach, R.; Chizhov, I.; Ataka, K.; Heberle, J.; Engelhard, M.; Bamberg, E. Proteorhodopsin is a light-driven proton pump with variable vectoriality. *J. Mol. Biol.* **2002**, *321*, 821-838.

(72) Hammes-Schiffer, S.; Iordanova, N. Theoretical studies of proton-coupled electron transfer reactions. *Biochim. Biophys. Acta* **2004**, *1655*, 29-36.

(73) Costentin, C. Electrochemical approach to the mechanistic study of proton-coupled electron transfer. *Chem. Rev.* **2008**, *108*, 2145-2179.

(74) Costentin, C.; Robert, M.; Saveant, J. M. Electrochemical concerted proton and electron transfers. Potential-dependent rate constant, reorganization factors, proton tunneling and isotope effects. *J. Electroanal. Chem.* **2006**, *588*, 197-206.

(75) Huynh, M. H. V.; Meyer, T. J. Proton-coupled electron transfer. *Chem. Rev.* **2007**, *107*, 5004-5064.

(76) Mayer, J. M.; Rhile, I. J. Thermodynamics and kinetics of proton-coupled electron transfer: Stepwise vs. concerted pathways. *Biochim. Biophys. Acta* **2004**, *1655*, 51-58.

(77) Hatcher, E.; Soudackov, A. V.; Hammes-Schiffer, S. Proton-coupled electron transfer in soybean lipoxygenase. *J. Am. Chem. Soc.* **2004**, *126*, 5763-5775.

(78) Knapp, M. J.; Rickert, K.; Klinman, J. P. Temperature-dependent isotope effects in soybean lipoxygenase-1: Correlating hydrogen tunneling with protein dynamics. *J. Am. Chem. Soc.* **2002**, *124*, 3865-3874.

(79) Rhile, I. J.; Mayer, J. M. One-electron oxidation of a hydrogen-bonded phenol occurs by concerted proton-coupled electron transfer. *J. Am. Chem. Soc.* **2004**, *126*, 12718-12719.

(80) Shukla, D.; Young, R. H.; Farid, S. Reducing power of photogenerated alpha-hydroxy radicals: Proton-coupled electron transfer. *J. Phys. Chem. A* **2004**, *108*, 10386-10394.

(81) Weatherly, S. C.; Yang, I. V.; Thorp, H. H. Proton-coupled electron transfer in duplex DNA: Driving force dependence and isotope effects on electrocatalytic oxidation of guanine. *J. Am. Chem. Soc.* **2001**, *123*, 1236-1237.

(82) Bordwell, F. G.; Cheng, J. P.; Ji, G. Z.; Satish, A. V.; Zhang, X. M. Bond-dissociation energies in DMSO related to the gas-phase. *J. Am. Chem. Soc.* **1991**, *113*, 9790-9795.

(83) Schowen, K. B.; Schowen, R. L. Solvent isotope effects of enzyme systems. *Methods Enzymol.* **1982**, *87*, 551-606.

(84) Schowen, R. L. In *Mechanistic Principles of Enzyme Activity*; Liebman, J. F., Greenberg, A., Eds.; VCH Publishers: New York, 1988, p 119-168.

(85) Venkatasubban, K. S.; Schowen, R. L. The proton inventory technique. *CRC Crit. Rev. Biochem.* **1984**, *17*, 1-44.

(86) Elrod, J. P.; Hogg, J. L.; Quinn, D. M.; Venkatasubban, K. S.; Schowen, R. L. Protonic reorganization and substrate structure in catalysis by serine proteases. *J. Am. Chem. Soc.* **1980**, *102*, 3917-3922.

(87) Matta, M. S.; Vo, D. T. Proton inventory of the 2nd step of ribonuclease catalysis. *J. Am. Chem. Soc.* **1986**, *108*, 5316-5318.

(88) Venkatasubban, K. S.; Silverman, D. N. Carbon dioxide hydration activity of carbonic anhydrase in mixtures of water and deuterium oxide. *Biochemistry* **1980**, *19*, 4984-4989.

Chapter 2

Proton-Coupled Electron Transfer and Tyrosine D of Photosystem II

by

David L. Jenson, Amaris Evans and Bridgette A. Barry

School of Chemistry and Biochemistry and the Parker H. Petit Institute for Bioengineering and Bioscience, Georgia Institute of Technology, Atlanta, Georgia 30332

Reprinted with permission from the American Chemical Society

Jenson, D. L.; Evans, A.; Barry B. A. "Proton-Coupled Electron Transfer in Tyrosine D of Photosystem II." *J. Phys. Chem. B* **2007**, *111*, 12599-12604.

2.1 Abstract

Photosystem II (PSII) is a photosynthetic reaction center that oxidizes water and reduces bound plastoquinone. PSII electron transfer is mediated by two redox-active tyrosine residues. One of these residues, tyrosine D (Y_D), has been assigned as Tyr160 of the D2 polypeptide by site-directed mutagenesis and isotopic labeling. Previous spectroscopic evidence has established that His189 in the D2 subunit forms a hydrogen bond with $Y_D^{\bullet}$ and donates a proton to $Y_D^{\bullet}$ when the radical is reduced. However, the mechanism of this reaction has not been elucidated. In this report, EPR spectroscopy and ^2H_2O solvent exchange were used to investigate the pL (where pL is either p^1H or p^2H) dependence of the $Y_D^{\bullet}$ reduction rate. The kinetic isotope effect (KIE), induced by solvent exchange, was also measured as a function of pL. Under the conditions employed, the reduction of $Y_D^{\bullet}$ is attributed to recombination with the Q_A^- plastoquinone acceptor of PSII. The kinetic data were fit with a biexponential function. The majority, slow phase exhibited a pL-dependent rate constant, with a minimum at pL 7.0. Solvent exchange gave significant KIE at values between pL 5.5 and 8.0. In particular, at high pL ($\geq$ 7.5), the values of the KIE were determined to be 2.1 ± 0.6 and 2.4 ± 0.5. These values are consistent with a coupled electron and proton reaction, which occurs with a single kinetic step at pL values $\geq$ 7.5. The lower KIE values and the rate acceleration observed at low pL, may be consistent with a change of mechanism, in which the protonation of $Y_D^{\bullet}$ occurs first, followed by rate-limiting electron transfer. The more modest rate acceleration in rate at high pL values is attributed to a small, pL induced change in the distance between $Y_D^{\bullet}$ and Q_A^-.

2.2 Introduction

PSII is a thylakoid membrane protein complex that carries out the light-catalyzed oxidation of H_2O. Photoexcitation results in the oxidation of a chlorophyll (chl) donor and the sequential reduction of two quinone acceptors, Q_A and Q_B, on the stromal side of PSII. Q_B functions as a two electron-two proton acceptor, while Q_A accepts only a single electron and is not protonated during the electron transfer reaction. H_2O oxidation occurs on the lumenal side of PSII in the oxygen-evolving complex (OEC), a $Ca[Mn]_4$ metallocluster.[1-4]

PSII is a prototypical system for the study of redox-active amino acids, because two redox-active tyrosine residues are involved in light-induced electron transfer reactions.[5] Y_Z (Tyr 161 in the D1 subunit) mediates electron transfer events between the OEC and the chl donor.[6-8] The oxidized form, $Y_Z^{\bullet}$, is a neutral radical, which decays on the microseconds to milliseconds time scale.[9,10] Y_D (Tyr 160 in the D2 subunit) influences, but is not required for, water oxidizing activity and forms a stable, neutral radical, $Y_D^{\bullet}$, which decays on the minutes to hours time scale, depending on preparation.[5,11-13] At pH values below the pK_a of the singlet tyrosine state (p$K_a \sim 10$), the Y_D and Y_Z phenolic side chains are most likely in the protonated form. Because the pK_a of the phenolic proton is dramatically altered (p$K_a < 0$) by radical formation,[14] redox-active tyrosines function in proton-coupled electron transfer reactions in enzymes. Differences in the mechanism of these reactions may contribute to observed alterations in midpoint potential and electron transfer rate, when Y_D and Y_Z are compared.

PSII structures are available at 3.8-3.0 Å resolution.[1-4] In the 3.0 Å structure, Y_D is within hydrogen bonding distance of a histidine, His189 in the D2 subunit (Figure

1A).[4] ESE-ENDOR spectroscopy has detected a hydrogen bond between His189D2 and $Y_D^{\bullet}$.[15] At pH 7.5, difference FT-IR spectroscopy has shown a perturbation of the His189D2 NH stretching vibrations, which is consistent with a proton transfer reaction from the protonated imidazole side chain of His189D2 to $Y_D^{\bullet}$.[16] Further, a mutation at His189D2 slowed the rate of $Y_D^{\bullet}$ reduction; chemical complementation with imidazole accelerated the reduction rate in this mutant at pH 7.5.[16] These previous studies have established that His189D2 interacts with $Y_D/Y_D^{\bullet}$ and acts as a proton acceptor/donor.

To obtain more information concerning the mechanism of proton-coupled electron transfer, we have performed solvent isotope exchange and measured the kinetic isotope effect on $Y_D^{\bullet}$ reduction. $Y_D^{\bullet}$ can be detected independently of $Y_Z^{\bullet}$ and other PSII electron donors by EPR spectroscopy.

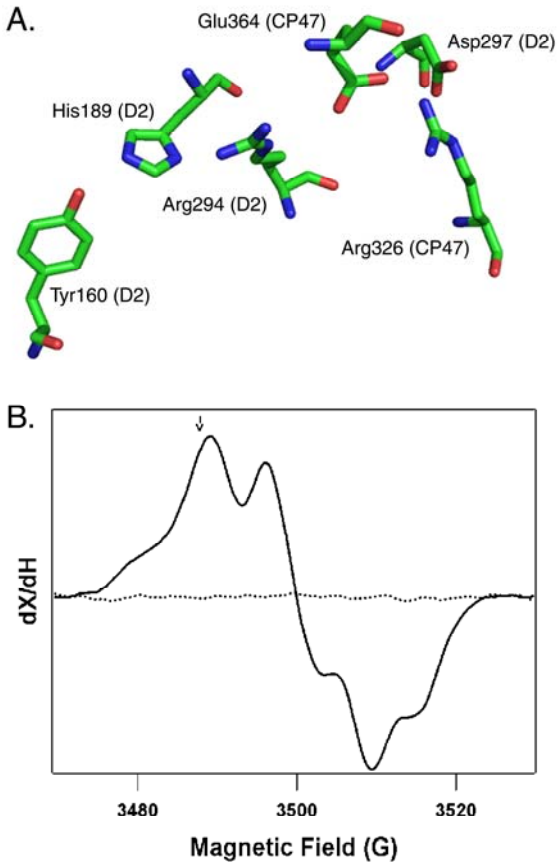

Figure 1. (A) Titrable amino acid side chains near Y_D in the 3.0 Å[4] PSII structure. Only titrable amino acids are shown. (B) Field swept, room temperature EPR[13,17] spectrum of $Y_D^{\bullet}$, (solid line) showing the field used for kinetic data acquisition (arrow) and a buffer blank (dotted line). Experimental conditions: frequency, 9.8 GHz; time constant, 1.3 s; conversion time, 164 ms; modulation amplitude, 2.0 G; modulation frequency, 100 kHz; microwave power, 2.5 mW; total data acquisition time, 9 min; concentration, 1.9 mg chl $(mL)^{-1}$, pH 6.0 SMN buffer.

2.3 Materials and Methods

PSII was isolated from market spinach.[18] The oxygen evolution rates were > 650 μmol O_2/(mg chl h)$^{-1}$.[19] PSII was depleted of the OEC, as well as the 18-, 24- and 33-kDa extrinsic polypeptides, by treatment with Tris buffer (final concentration, 0.8 M Tris-HCl and 2.0 mM tetrasodium EDTA) at pH 8.0.[20] The PSII samples were pooled and were exchanged into ^1H_2O or ^2H_2O at pL 5.0, 5.5, 6.0, 6.5, 7.0, 7.5 and 8.0 by dialysis.

^2H_2O was purchased from Cambridge Isotope Laboratories (99% ^2H enrichment, Andover, CA). The p^2H of ^2H_2O buffers is reported as the uncorrected meter reading,[21] because the characteristic, small solvent isotope effects on weak acid pK_a values are approximately canceled by the ^2H_2O-induced change in response of the glass pH electrode.[22] The p^2H was adjusted with NaO^2H (Cambridge Isotopes, 99.5% ^2H enrichment). Dialysis employed a 6-8 kDa cutoff membrane (Spectrum, Laguna Hills, CA), and two rounds of dialysis (9 and 16 h each) into 500 mL (1:50 dilution) of the appropriate buffer were performed. The pL 5.5, 6.0 and 6.5 samples were dialyzed against 0.40 M sucrose, 50 mM MES-NaOL, 15 mM NaCl (SMN). The pL 7.5 and 8.0 samples were dialyzed against 0.40 M sucrose, 50 mM HEPES-NaOL, 15 mM NaCl (SHN). Two pL 7.0 samples were prepared, one in SMN buffer and the other in SHM buffer. After dialysis, the samples were stored at -70 ºC in 500 μL aliquots.

To monitor the extent of deuterium exchange as a function of pL, ATR/FT-IR spectroscopy was conducted using a Bruker IFS-66v/s FT-IR spectrometer outfitted with a Bruker BIOATR II cell (germanium internal reflection element) and a photovoltaic detector (Bruker part #D317/3). PSII samples were 20 μL, and 100 scans were acquired for each FT-IR sample. The spectrum of each buffer at the appropriate pL was subtracted from the PSII spectrum. FT-IR conditions were as follows: resolution = 4 cm^{-1}; aperture = 8 mm; scanner velocity = 20.0 kHz; acquisition mode = double sided, forward-backward; phase resolution = 16; phase correction mode = Mertz; apodization function = Happ-Genzel; zero filling factor = 4. The method of Rath et al. was used to quantitate the amount of peptide deuterium exchange. The fractional amount of protein unexchanged,

f, was determined by the relation $f = w'/w$, where $w = (A_{\text{amide II}}/A_{\text{amide I}})$ in ^1H_2O and $w' = (A_{\text{amide II}}/A_{\text{amide I}})$ in ^2H_2O-dialyzed samples.[23,24]

EPR[13,16,17,25] analysis was conducted at room temperature using a Bruker EMX spectrometer (Billerica, MA) equipped with a Bruker HS4119 high sensitivity cavity. All experiments utilized a quartz EPR flat cell (Wilmad-Lab Glass, Buena, NJ). The cavity temperature was maintained with a stream of dry nitrogen. Samples contained 10 μM (3-(3,4-dichlorophenyl)-1,1-dimethylurea (DCMU) to inhibit Q_B^- formation. The stock DCMU solution was dissolved in absolute ethanol, and the total concentration of ethanol in the EPR sample was < 0.5%. When added, potassium ferricyanide (final concentration, 3 mM) and potassium ferrocyanide (final concentration, 3 mM) were dissolved as stock solutions in the appropriate buffer just before the experiment. The chlorophyll concentration, which is proportional to PSII reaction center concentration,[26] of each sample was measured before the EPR measurements. $Y_D^\bullet$ was generated by flashing 120 times at 1 Hz with the 532 nm second harmonic of a Continuum Surelite III Nd:YAG laser (Santa Clara, CA). The laser beam was expanded with use of a cylindrical lens. The laser intensity was 50 ± 1 mJ/cm^2. $Y_D^\bullet$ formation kinetics are on the nanoseconds to microseconds time scale[27] and cannot be resolved in our EPR experiments. The kinetics of $Y_D^\bullet$ reduction were monitored with no contribution from $Y_Z^\bullet$ decay, because photo-induced $Y_Z^\bullet$ (τ = 200 ms)[17] decayed in the 56 s between laser excitation and the beginning of data analysis. Kinetic traces were fit with IGOR Pro software (Lake Osawego, OR). Except where noted, three sets of kinetics were recorded on each sample, and the decay kinetics were found to be comparable in each set. After the kinetic experiments, the field-swept EPR signal was recorded and was shown to have a normal $Y_D^\bullet$ lineshape (for

example, see Figure 1B). A microwave power saturation curve was obtained on a representative PSII sample, and the microwave powers used in the field-swept and kinetic experiments were shown to be non-saturating. Kinetic experiments were performed with blanks, which contained all reactants except PSII, at each pL value.

2.4 Results and Discussion

To investigate the mechanism of $Y_D^{\bullet}$ reduction, solvent isotope exchange was performed at pL values between 5.5 and 8.0. PSII[18] samples were stable at these pH values and were treated[20] to remove the OEC, which acts as an electron donor to $Y_D^{\bullet}$. $Y_D^{\bullet}$ was generated by 532 nm photoexcitation from a doubled Nd:YAG laser,[13,17] and its subsequent decay via reduction was detected by EPR spectroscopy (Figure 1B and Figure 2). This dialysis method has been shown to substitute imidazole into the $Y_D^{\bullet}$ pocket in a PSII site-directed mutant.[16] Magnetic resonance studies have established a ~9 hour halftime for exchange in the Y_D pocket. [28] Our total dialysis times are 25 hour and then samples are frozen, thawed, and assayed in ^2H_2O. Therefore, ^2H exchange in the $Y_D^{\bullet}$ pocket is expected to be facile at all pH values under these conditions. In agreement with these expectations, the extent of exchange, as monitored by FT-IR spectroscopy, was shown to be relatively pL invariant (Figure 3 and Figure 4). The overall extent of exchange (~50%) is high for a hydrophobic membrane protein.[23]

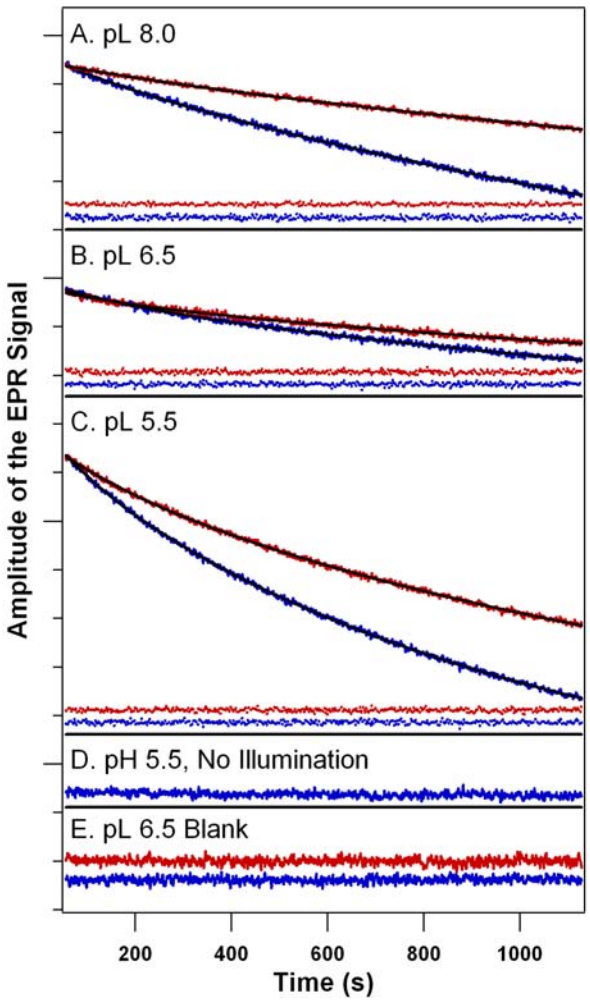

Figure 2. Kinetic data, associated with the reduction of $Y_D^{\bullet}$ by Q_A^-, in ^1H_2O (blue, solid lines) and ^2H_2O buffers (red, solid lines). The corresponding fits (black) and residuals (dotted) are shown in A-C. The data were fit from 56 to 1128 s. The traces shown in panels A-E were offset on the y-axis for presentation purposes. The ^1H_2O and ^2H_2O kinetic traces were also adjusted to give the same amplitude at t = 56 for presentation. (A) pL 8.0 in HEPES buffer; (B) pL 6.5 in MES buffer; (C) pL 5.5 in MES buffer; (D) pH 5.5 in MES buffer, no illumination control; (E) pL 6.5 blank in MES buffer containing DCMU, ferricyanide, and ferrocyanide, but excluding PSII. Experimental conditions: frequency, 9.8 GHz; time constant, 1.3 s; conversion time, 164 ms; modulation amplitude, 5.0 G; modulation frequency, 100 kHz; microwave power, 6.4 mW; concentration, 1.7-2.1 mg chl $(mL)^{-1}$.

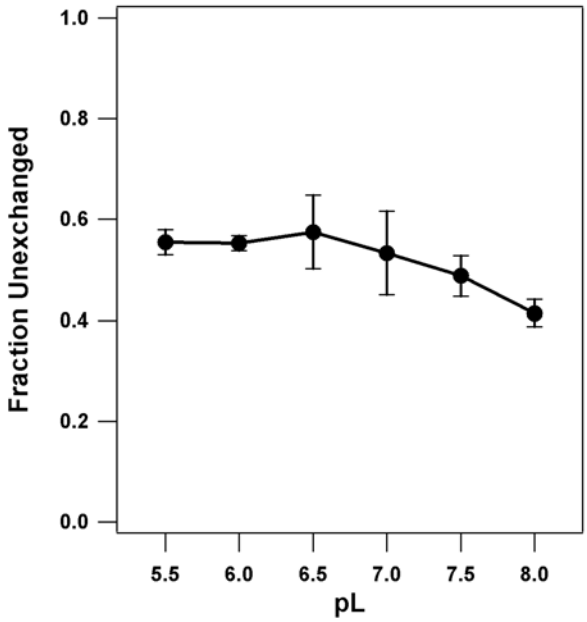

Figure 3. The PSII fraction unexchanged with $^{2}H_2O$ as a function of pL. The total fraction of unexchanged peptide groups was calculated from the ATR/FT-IR spectrum as previously described.[23,24] The data point at pL 7.0 was in SHN buffer. See Materials and Methods for details. An example of the FT-IR absorption spectrum is presented in Figure 4.

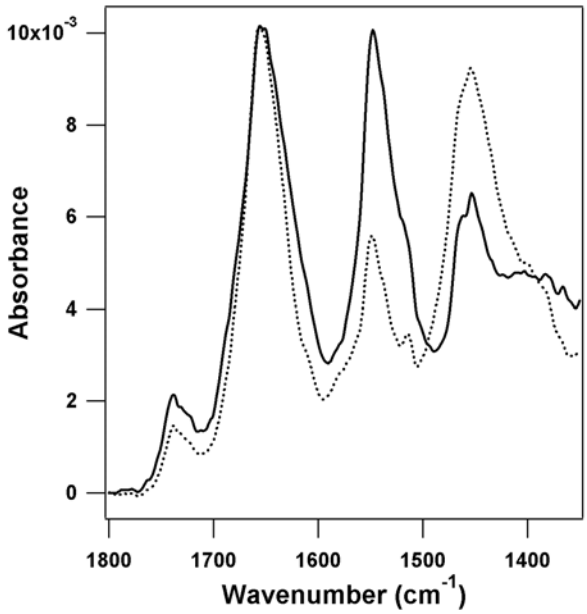

Figure 4. Representative ATR/FT-IR absorption spectra, used to quantitate the extent of deuterium exchange in PSII samples. The data are normalized to the amide I band intensity at ~1650 cm^{-1} and were acquired at pL 6.0. The solid line is the absorption in $^{1}H_2O$. The dotted line is the absorption in $^{2}H_2O$.

Figure 2 presents representative kinetic traces obtained at pL (A) 8.0, (B) 6.5, and (C) 5.5 in $^{1}H_2O$ (blue) and $^{2}H_2O$ (red) buffers. The fits to the data are shown superimposed on the data (black lines), and the residuals are shown at the bottom of each panel (dotted lines). Figure 2D shows that no appreciable decay was observed in a dark-adapted sample, which was not flashed with the laser. Figure 2E is a representative blank, showing that no kinetic trace was obtained in the absence of PSII.

EPR samples contained 3-(3,4-dichlorophenyl)-1,1-dimethylurea (DCMU), which inhibits electron transfer reactions to the protonatable Q_B site.[29] Because Q_A reduction does not result in the protonation of the quinone,[30] this precaution insures that any observed solvent isotope effects are attributable directly to redox reactions involving $Y_D^{\bullet}$. However, control experiments showed that the presence of DCMU had no detectable effect on the amplitude of $Y_D^{\bullet}$ or the kinetics of its decay, which is consistent with a non-functional Q_B site in these PSII preparations (Table 1 and Table 2).

Table 1. Rate constants and kinetic isotope effects (KIE) for the majority kinetic phase of $Y_D^{\bullet}$ reduction, as assessed by EPR spectroscopy[a]

DCMU	Ferricyanide/ Ferrocyanide	pL	Isotope/Buffer	Rate Constant[b] (10^{-4} s^{-1})	Amplitude (%)[b]	KIE[c]
+	+	5.5	H_2O/MES	10.3 ± 0.8	94 ± 3	1.7 ± 0.4
+	+		D_2O/MES	6.10 ± 1.45	89 ± 3	
+	+	6.0	H_2O/MES	2.17 ± 0.27	91 ± 1	1.2 ± 0.2
+	+		D_2O/MES	1.89 ± 0.27	95 ± 4	
+	+	6.5	H_2O/MES	1.42 ± 0.23	94 ± 2	1.3 ± 0.2
+	+		D_2O/MES	1.10 ± 0.08	95 ± 1	
+	+	7.0	H_2O/MES	1.45 ± 0.24	96 ± 2	2.0 ± 0.4
+	+		D_2O/MES	0.72 ± 0.10	96 ± 2	
+	+	7.0	H_2O/HEPES	1.26 ± 0.17	97 ± 2	1.4 ± 0.3
+	+		D_2O/HEPES	0.92 ± 0.15	97 ± 3	
+	+	7.5	H_2O/HEPES	1.78 ± 0.30	95 ± 1	2.1 ± 0.6
+	+		D_2O/HEPES	0.84 ± 0.20	98 ± 1	
+	+	8.0	H_2O/HEPES	2.78 ± 0.35	96 ± 1	2.4 ± 0.5
+	+		D_2O/HEPES	1.17 ± 0.20	98 ± 1	
+	-	7.0[d]	H_2O/HEPES	1.52 ± 0.06	95 ± 1	NA
+	-	8.0[d]	H_2O/HEPES	3.07 ± 0.11	98 ± 2	NA
-	+	5.5[e]	H_2O/MES	9.13 ± 0.67	79 ± 4	NA
-	+	6.5[e]	H_2O/MES	1.39 ± 0.25	91 ± 1	NA
+	+	6.0[f]	H_2O/MES	2.17 ± 0.53	94 ± 3	NA

[a]Means are reported plus/minus one standard deviation. The means are the average of three measurements on three-six samples, and the EPR samples contained 10 μM DCMU, 3 mM potassium ferricyanide, and 3 mM potassium ferrocyanide, except where noted. [b]Majority, slow phase amplitudes and rate constants obtained from a biexponential fit to the EPR kinetic data. Fits were performed with Igor Pro software (Wavemetrics, Lake Oswego, OR). The fast phase rate constants, fast phase amplitudes, and the amplitudes of the nondecaying component are presented in Table 2. The mean χ^2 values for the fits were 2.0 ± 0.1 x 10^7. Monoexponential functions gave a less reliable fit to the data, as assessed by the χ^2 value. [c]Ratio of the rate constant measured in ^1H_2O to the rate constant in ^2H_2O. NA is not applicable. [d]Samples contained only 10 μM DCMU, and the means are the average of three measurements on two samples. [e]Samples contained no DCMU, but 3 mM ferricyanide/ferrocyanide. [f]Samples were not dialyzed.

Table 2. Summaries of the minority (fast) phase amplitudes, rate constants, and kinetic isotope effects, as well as the amplitude of the non-decaying phase (C_0), for $Y_D^{\bullet}$ decay, as assessed by EPR spectroscopy[a]

DCMU	Ferricyanide/ Ferrocyanide	pL	Isotope/Buffer	Rate Constant[b] (10^{-3} s^{-1})	Amplitude (%)[b]	Non-Decaying Component (%)[b]	KIE[c]
+	+	5.5	H_2O/MES	8.72 ± 0.70	8 ± 3	ND	1.6 ± 0.2
+	+		D_2O/MES	5.33 ± 0.51	10 ± 2	ND	
+	+	6.0	H_2O/MES	6.63 ± 1.20	8 ± 1	ND	1.2 ± 0.2
+	+		D_2O/MES	5.42 ± 0.22	6 ± 1	ND	
+	+	6.5	H_2O/MES	4.38 ± 0.75	6 ± 1	ND	0.8 ± 0.2
+	+		D_2O/MES	5.49 ± 1.40	5 ± 1	ND	
+	+	7.0	H_2O/MES	4.84 ± 0.70	5 ± 1	ND	1.4 ± 0.5
+	+		D_2O/MES	3.55 ± 1.09	5 ± 2	ND	
+	+	7.0	H_2O/HEPES	4.93 ± 0.43	5 ± 1	ND	1.1 ± 0.2
+	+		D_2O/HEPES	4.50 ± 0.55	4 ± 1	ND	
+	+	7.5	H_2O/HEPES	5.38 ± 1.29	4 ± 1	ND	0.9 ± 0.6
+	+		D_2O/HEPES	5.96 ± 3.40	3 ± 1	ND	
+	+	8.0	H_2O/HEPES	4.49 ± 0.92	5 ± 1	ND	1.0 ± 0.4
+	+		D_2O/HEPES	4.70 ± 1.97	3 ± 1	ND	
+	-	7.0[d]	H_2O/HEPES	5.00 ± 0.01	4 ± 1	ND	NA
+	-	8.0[d]	H_2O/HEPES	4.58 ± 0.01	4 ± 1	ND	NA
-	+	5.5[e]	H_2O/MES	7.72 ± 4.61	15 ± 2	6 ± 6	NA
-	+	6.5[e]	H_2O/MES	5.61 ± 1.03	7 ± 1	ND	NA
+	+	6.0[f]	H_2O/MES	5.68 ± 2.84	5 ± 1	ND	NA

[a]Means are reported plus/minus one standard deviation. The means are the average of three measurements on three-six samples, and the EPR samples contained 10 μM DCMU, 3 mM potassium ferricyanide, and 3 mM potassium ferrocyanide, except where noted. [b]Fast phase amplitudes, fast phase rate constants, and the amplitude of the non-decaying component, obtained from a biexponential fit to the EPR kinetic data. Fits were performed with Igor Pro software (Wavemetrics, Lake Oswego, OR). The slow phase rate constants and amplitudes are presented in paper. The mean χ^2 values for the fits were 2.0 ± 0.1 x 10^7. Monoexponential functions gave a less reliable fit to the data, as assessed by the χ^2 value. When the amplitude was less than or equal to 1%, the amplitude is reported as not detected (ND). [c]Ratio of the rate constant measured in ^1H_2O to the rate constant in ^2H_2O. NA is not applicable. [d]Samples contained only 10 μM DCMU, and the mean is the average of three measurements on two samples. [e]Samples contained no DCMU, but 3 mM ferricyanide/ferrocyanide. [f]Samples were not dialyzed.

The total amplitude of the 532 nm flash-induced signal at t = 0 was found to be independent of pL (data not shown) after correction for the reaction center (chl) concentration. The total amplitude was also found to be indistinguishable from the amplitude observed in the $Y_D^{\bullet}$ EPR signal, acquired under illumination. Previous work, using a spin standard, has shown that our PSII preparations exhibit 0.9 $Y_D^{\bullet}$ spin per reaction center.[13] These control experiments support the interpretation that the kinetic experiments interrogate the majority of the $Y_D^{\bullet}$ population. In addition, the long dialysis itself was shown to have no significant effect on the rate of $Y_D^{\bullet}$ decay (Table 1 and Table 2).

At all pL values examined, the kinetics of $Y_D^{\bullet}$ reduction could be fit with a biexponential function, $C_0 + C_1\exp(-k_1t) + C_2\exp(-k_2t)$ (Table 1, Table 2 and Figure 2). A summary of derived values for the slow, majority phase is presented in Table 1. The slow phase represented the majority of the amplitude at pL values between 5.5 and 8.0 (Table 1). Summaries of the minority (fast) phase amplitudes, rate constants, and kinetic isotope effects, as well as the amplitude of the non-decaying phase (C_0), are given in Table 2 for each pL value. The fast phase was $\leq$ 15% of the amplitude and is attributed to a small percentage of PSII reaction centers in an altered conformation, in which ferrocyanide is a facile electron donor.

The slow phase showed pL-dependent rate constants, with a minimum at ~pH 7.5, both in ^1H_2O (Figure 5, black) and ^2H_2O buffers (Figure 5, blue). The kinetics of $Y_D^{\bullet}$ decay did not depend on the choice of buffering agent, as shown by a comparison of MES- and HEPES-buffered samples at pL 7.0 (Table 1 and Table 2). The rate of $Y_D^{\bullet}$ reduction did not depend on the presence of an electron donor and acceptor, potassium

ferrocyanide and potassium ferricyanide (Table 1 and Table 2). Therefore, the reduction of $Y_D^{\bullet}$ is attributed to an internal recombination event[31] between $Y_D^{\bullet}$ and Q_A^{-}.

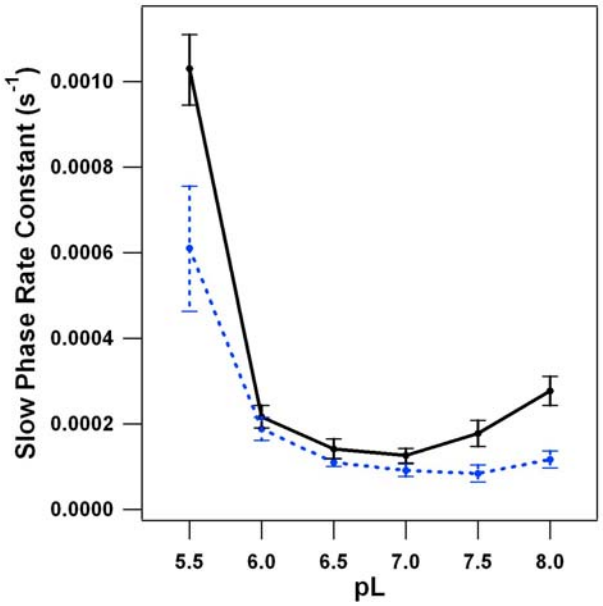

Figure 5. pL dependence of the majority, slow phase of $Y_D^{\bullet}$ reduction, as assessed by EPR[13,17] spectroscopy, in ^1H_2O- (black) and ^2H_2O- (blue) buffers. The data are taken from Table 1. Examples of the data are shown in Figure 2. Error bar represent ± 1 standard deviation.

Table 1 and Figure 6 present the solvent kinetic isotope effect (KIE) determined at each pL value for the majority kinetic phase. Significant solvent isotope effects were observed. At pL 7.5 and 8.0, the KIEs are 2.1 ± 0.6 and 2.4 ± 0.5, respectively. Three distinct proton-electron transfer mechanisms (Scheme 1) are possible for $Y_D^{\bullet}$ reduction.[32-34] The first possible mechanism is rate-limiting electron transfer to $Y_D^{\bullet}$, to yield anionic Y_D^{-}, followed by fast proton transfer to give the product, Y_D (ETPT). A second possible mechanism is a pre-equilibrium proton transfer to give the cation radical, $Y_DH^{+\bullet}$, followed by electron transfer to give Y_D (PTET). A third possible mechanism is the concerted transfer of an electron and a proton to $Y_D^{\bullet}$ in one kinetic step (CPET). Other

mechanisms involve sequential electron and proton transfer reactions in which proton transfer is the slow, rate-limiting step. However, these slow proton transfer mechanisms seem unlikely given the slow rate of $Y_D^{\bullet}$ reduction and the generally fast rate of biological proton transfer reactions.[35,36]

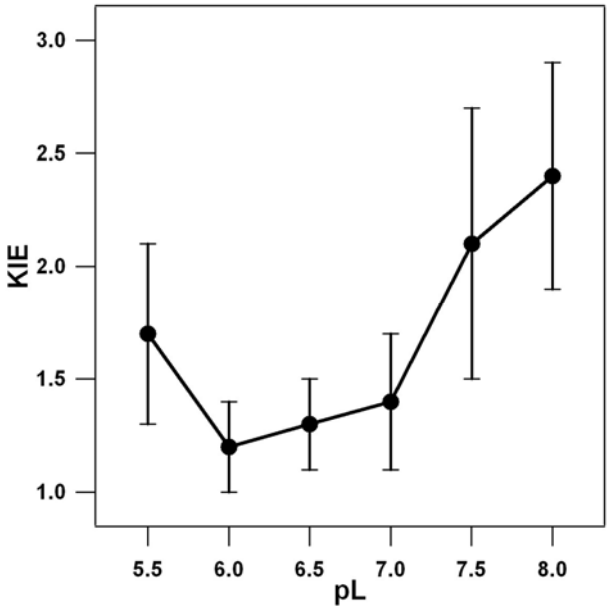

Figure 6. pL dependence of the solvent isotope effect on the slow phase of $Y_D^{\bullet}$ reduction. The data are taken from Table 1. Error bars represent ± 1 standard deviation.

Scheme 1

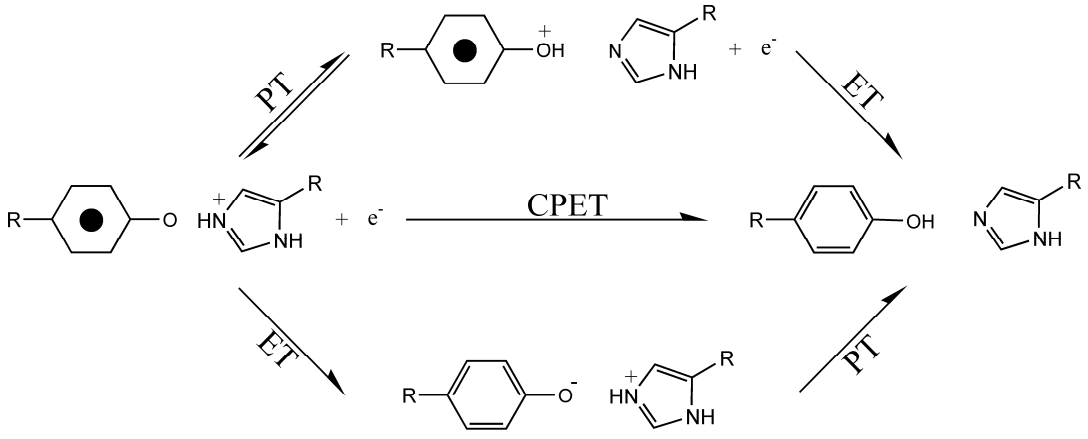

The first three possible mechanisms can be distinguished by the magnitude of the solvent isotope effect on the rate of $Y_D^{\bullet}$ reduction, which is expected to show only a small (< 1.3) kinetic isotope effect for ETPT mechanism one, but a more significant kinetic isotope effect (greater than or equal to 1.6) for CPET mechanism three.[34,37-48] Mechanism two would show only a small equilibrium isotope effect (~0.5 ΔpK_A) in ^2H_2O buffers[22,34] and also predicts a pH-dependent rate. In this pre-equilibrium type of proton transfer, the rate constant will increase by a factor of 10 per pH unit, as decreasing pH approaches the pK_a of $Y_D^{\bullet}$.[35,36]

On the basis of the discussion above, the substantial kinetic isotope effects at high pL (2.1 ± 0.6 and 2.4 ± 0.5, Figure 6 and Table 1) provide support for a mechanism in which electron and proton transfer to $Y_D^{\bullet}$ occur by a concerted CPET pathway. This reaction is an example of a concerted proton transfer reaction in which the electron and proton come from different donors, Q_A^- and His189D2, respectively. Note that the small rate acceleration observed at pL 8.0 is significant, given the standard deviation of the measurements (Table 1 and Figure 5). This acceleration of the electron transfer rate is not explicable as an effect on titrable groups in the environment of $Y_D^{\bullet}$ (Figure 1A). Therefore, we attribute this change to a pH-induced conformational change, which slightly increases the rate constant for the $Q_A^-/Y_D^{\bullet}$ recombination reaction at high pL values.

Figure 5 shows that as the pL decreases below 7.0, an acceleration in the rate of $Y_D^{\bullet}$ reduction is observed. The KIEs also show an overall decrease (Figure 6). This result may be consistent with a low pL mechanism in which protonation of $Y_D^{\bullet}$ occurs first, followed by rate-limiting electron transfer.[34] For this pre-equilibrium proton transfer

mechanism, a 10-fold rate acceleration per pL unit is expected as the pL approaches the pK_a of $Y_D^{\bullet}$ (assumed to be ~ 0 in PSII). A 5-fold rate increase was observed when pL 5.5 and 6.0 were compared (Table 1). At pL 5.0, a unique fit to the kinetic data was not found (data not shown). However, comparing the half times, the rate increased by additional factor of 6-9, when data at pL 5.0 and 5.5 were compared. This large rate increase may be caused by a PTET mechanism and by the pH dependence of the tyrosine standard reduction potential, which increases linearly below pH 10 with a slope of 59 mV/pH unit.[49,50] For a pre-equilibrium proton transfer mechanism, the observed rate is the product of K, the equilibrium constant for proton transfer from His189D2 to $Y_D^{\bullet}$, and the intrinsic electron transfer rate to $Y_D^{\bullet}$. If the pK_a difference between His189D2 and $Y_D^{\bullet}$ is assumed to be approximately 8, then the observed rate constant predicts an intrinsic electron transfer rate on the microsecond time regime.

Scheme 2 shows that changes in His189 pK_a (reactions C and D) and tyrosine oxidation state (reactions A and B) are thermodynamically linked. To explain our results, we assume that the protonated imidazole side chain of His189D2 acts as a proton donor to $Y_D^{\bullet}$ from pL 5.5 to 8.0. This is possible if the pK_a of its imidazole side chain increases when the radical state is formed, thereby favoring the protonated state of His189D2. Precedent for such an increase in histidine pK_a has been obtained from studies of a model β-hairpin peptide, in which a tyrosine and histidine side chain are π-π stacked, but are not hydrogen bonded.[50] The pK_a shift observed in that case was one pH unit and was attributed to a change in the electrostatic map of tyrosine, when the aromatic ring is oxidized. A concomitant ~50 mV decrease in tyrosine redox potential was also observed.[50] Similarly, to act as a proton acceptor from Y_D over the pL range from 5.5 to

8.0, the pK_a of His189D must be substantially decreased relative that of free imidazole. The environmental effects, which cause these pK_a shifts, have not as yet been elucidated.

Scheme 2

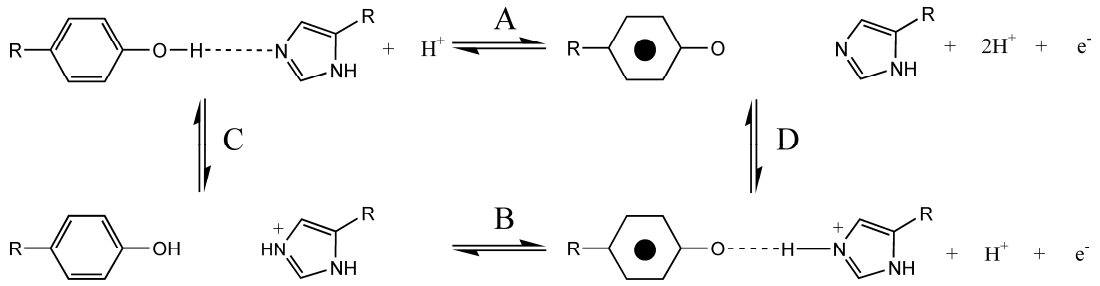

Previous work has identified CPET mechanisms in enzymes and model compounds. In lipoxygenase, CPET has been proposed to occur with a proton tunneling mechanism, giving rise to a large (81) primary isotope effect on the reaction.[41,44,45] For Y_Z, there are conflicting interpretations in the literature. A coupled proton-electron transfer mechanism has been proposed for linked tyrosine-histidine model compounds.[32,38,51] Similarly, the mechanism of Y_Z oxidation has been attributed to a CPET reaction,[47] but other authors have suggested a gated reaction in which the reaction rate is governed by histidine deprotonation[28] and a consecutive PTET reaction.[52] Our future work will use solvent isotope effects to compare the mechanism of $Y_Z^{\bullet}$ and $Y_D^{\bullet}$ reduction.

2.5 Acknowledgment

This work was supported by the National Institutes of Health, GM43273 (B. A. B.), and by the National Science Foundation Research Experience for Undergraduates in Chemistry and Biochemistry at Georgia Tech, Grant 0552722 (A. E.).

2.6 References

(1) Zouni, A.; Witt, H.-T.; Kern, J.; Fromme, P.; Krauß, N.; Saenger, W.; Orth, P. Crystal structure of photosystem II from *Synechococcus elongatus* at 3.8 Å resolution. *Nature* **2001**, *409*, 739-743.

(2) Kamiya, N.; Shen, J.-R. Crystal structure of oxygen-evolving photosystem II from *Thermosynechococcus vulcanus* at 3.7 Å resolution. *Proc. Natl. Acad. Sci. USA* **2003**, *100*, 98-103.

(3) Ferreira, K. N.; Iverson, T. M.; Maghlaoui, K.; Barber, J.; Iwata, S. Architecture of the photosynthetic oxygen-evolving center. *Science* **2004**, *303*, 1831-1837.

(4) Loll, B.; Kern, J.; Saenger, W.; Zouni, A.; Biesiadka, J. Towards complete cofactor arrangement in the 3.0 Å resolution structure of photosystem II. *Nature* **2005**, *438*, 1040-1044.

(5) Rutherford, A. W.; Boussac, A.; Faller, P. The stable tyrosyl radical in Photosystem II: why D? *Biochim. Biophys. Acta* **2004**, *1655*, 222-230.

(6) Debus, R. J.; Barry, B. A.; Sithole, I.; Babcock, G. T.; McIntosh, L. Directed mutagenesis indicates that the donor to P_{680}^{+} in photosystem II is Tyr-161 of the D1 polypeptide. *Biochemistry* **1988**, *27*, 9071-9074.

(7) Gerken, S.; Brettel, K.; Schlodder, E.; Witt, H. T. Optical characterization of the immediate donor to Chlorophyll a_{II}^{+} in O_2-evolving photosystem II complexes. *FEBS Lett.* **1988**, *237*, 69-75.

(8) Boerner, R. J.; Barry, B. A. Isotopic labeling and EPR spectroscopy show that a tyrosine residue is the terminal electron donor, Z, in manganese-depleted photosystem II preparations. *J. Biol. Chem.* **1993**, *268*, 17151-17154.

(9) Babcock, G. T.; Blankenship, R. E.; Sauer, K. Reaction kinetics for positive charge accumulation on the water side of chloroplast Photosystem II. *FEBS Lett.* **1976**, *61*, 286-289.

(10) Dekker, J. P.; Gorkom, H. J. V.; Brok, M.; Ouwehand, L. Optical characterization of photosystem II electron donors. *Biochim. Biophys. Acta* **1984**, *764*, 301-309.

(11) Barry, B. A.; Babcock, G. T. Tyrosine radicals are involved in the photosynthetic oxygen-evolving system. *Proc. Natl. Acad. Sci. USA* **1987**, *84*, 7099-7103.

(12) Debus, R. J.; Barry, B. A.; Babcock, G. T.; McIntosh, L. Site-specific mutagenesis identifies a tyrosine radical involved in the photosynthetic oxygen-evolving complex. *Proc. Natl. Acad. Sci. USA* **1988**, *85*, 427-430.

(13) Kim, S.; Ayala, I.; Steenhuis, J. J.; Gonzalez, E. T.; Razeghifard, M. R.; Barry, B. A. Infrared spectroscopic identification of the C-O stretching vibration associated with the tyrosyl $Z^{\bullet}$ and $D^{\bullet}$ radicals in photosystem II. *Biochim. Biophys. Acta* **1998**, *1366*, 330-354.

(14) Dixon, W. T.; Murphy, D. Determination of the acidity constants of some phenol radical cations by means of electron spin resonance. *J. Chem. Soc. London, Faraday Trans. II* **1976**, *72*, 1221-1229.

(15) Campbell, K. A.; Peloquin, J. M.; Diner, B. A.; Tang, X.-S.; Chisholm, D. A.; Britt, R. D. The τ-Nitrogen of D2 histidine 189 is the hydrogen bond donor to the tyrosine radical $Y_D^{\bullet}$ of photosystem II. *J. Am. Chem. Soc.* **1997**, *119*, 4787-4788.

(16) Kim, S.; Liang, J.; Barry, B. A. Chemical complementation identifies a proton acceptor for redox-active tyrosine D in photosystem II. *Proc. Natl. Acad. Sci. USA* **1997**, *94*, 14406-14412.

(17) Ma, C.; Barry, B. A. Electron paramagnetic resonance characterization of tyrosine radical, M^{+}, in site-directed mutants of photosystem II. *Biophys. J.* **1996**, *71*, 1961-1972.

(18) Berthold, D. A.; Babcock, G. T.; Yocum, C. F. A highly resolved, oxygen-evolving Photosystem II preparation from spinach thylakoid membranes. *FEBS Lett.* **1981**, *134*, 231-234.

(19) Barry, B. A. Tyrosyl radicals in photosystem II. *Methods Enzymol.* **1995**, *258*, 303-319.

(20) Yamomoto, Y.; Doi, M.; Tamura, N.; Nishimura, N. Release of polypeptides from highly active O_2-evolving photosystem II preparation by Tris treatment. *FEBS Lett.* **1981**, *133*, 265-268.

(21) Kim, S.; Sacksteder, C.; Barry, B. A. A reaction-induced FT-IR study of cyanobacterial Photosystem I. *Biochemistry* **2001**, *40*, 15384-15395.

(22) Schowen, K. B.; Schowen, R. L. Solvent isotope effects of enzyme systems. *Methods Enzymol.* **1982**, *87*, 551-606.

(23) Rath, P.; DeGrip, W. J.; Rothschild, K. J. Photoactivation of rhodopsin causes an increased hydrogen-deuterium exchange of buried peptide groups. *Biophys. J.* **1998**, *74*, 192-198.

(24) Sacksteder, C. A.; Bender, S. L.; Barry, B. A. Role for bound water and CH-pi aromatic interactions in photosynthetic electron transfer. *J. Am. Chem. Soc.* **2005**, *127*, 7879-7890.

(25) Kim, S.; Barry, B. A. The protein environment surrounding tyrosyl radicals $D^{\bullet}$ and $Z^{\bullet}$ in photosystem II: A difference FT-IR study. *Biophys. J.* **1998**, *74*, 2588-2600.

(26) Patzlaff, J. S.; Barry, B. A. Pigment quantitation and analysis by HPLC reverse phase chromatography: A characterization of antenna size in oxgyen-evolving photosystem II preparations from cyanobacteria and plants. *Biochemistry* **1996**, *35*, 7802-7811.

(27) Faller, P.; Debus, R. J.; Brettel, K.; Sugiura, M.; Rutherford, A. W.; Boussac, A. Rapid formation of the stable tyrosyl radical in photosystem II. *Proc. Natl. Acad. Sci. USA* **2001**, *98*, 14368-14373.

(28) Diner, B. A.; Force, D. A.; Randall, D. W.; Britt, R. D. Hydrogen bonding, solvent exchange, and coupled proton and electron transfer in the oxidation and reduction of redox-active tyrosine Y_Z in Mn-depleted core complexes of photosystem II. *Biochemistry* **1998**, *37*, 17931-17943.

(29) Mattoo, A. K.; Pick, U.; Hoffman-Falk, H.; Edelman, M. The rapidly metabolized 32,000-dalton polypeptide of the chloroplast is the "proteinaceous shield" regulating photosytem II electron transport and mediating diuron herbicide sensitivity. *Proc. Natl. Acad. Sci. USA* **1981**, *78*, 1573-1576.

(30) Rutherford, A. W.; Zimmerman, J. L. A new EPR signal attributed to the primary plastosemiquinone acceptor in photosystem II. *Biochim. Biophys. Acta* **1984**, *767*, 168-175.

(31) Demeter, S.; Goussias, C.; Bernat, G.; Kovacs, L.; Petrouleas, V. Participation of the g = 1.9 and g = 1.82 EPR forms of the semiquinome-iron complex Q_A^-/Fe^{2+} of photosystem II in the generation of the Q and C thermoluminescence bands, respectively. *FEBS Lett.* **1993**, *336*, 352-356.

(32) Sjodin, M.; Styring, S.; Akermark, B.; Sun, L. C.; Hammarstrom, L. Proton-coupled electron transfer from tyrosine in a tyrosine-ruthenium-tris-bipyridine complex: Comparison with Tyrosine(z) oxidation in photosystem II. *J. Am. Chem. Soc.* **2000**, *122*, 3932-3936.

(33) Reece, S. Y.; Nocera, D. G. Direct tyrosine oxidation using the MLCT excited states of rhenium polypyridyl complexes. *J. Am. Chem. Soc.* **2005**, *127*, 9448-9458.

(34) Rhile, I. J.; Markle, T. F.; Nagao, H.; DiPasquale, A. G.; Lam, O. P.; Lockwood, M. A.; Rotter, K.; Mayer, J. M. Concerted proton-electron transfer in the oxidation of hydrogen bonded phenols. *J. Am. Chem. Soc.* **2006**, *128*, 6075-6088.

(35) Graige, M. S.; Paddock, M. L.; Bruce, J. M.; Feher, G.; Okamura, M. Y. Mechanism of proton-coupled electron transfer for quinone (Q_B) reduction in reaction centers of *Rb*. *sphaeroides*. *J. Am. Chem. Soc.* **1996**, *118*, 9005-9016.

(36) Graige, M. S.; Paddock, M. L.; Feher, G.; Okamura, M. Y. Observation of the protonated semiquinone intermediate in isolated reaction centers from *Rhodobacter sphaeroides*: Implications for the mechanism of electron and proton transfer in proteins. *Biochemistry* **1999**, *38*, 11465-11473.

(37) Buhks, E.; Bixon, M.; Jortner, J. Deuterium isotope effects on outer sphere electron transfer reactions. *J. Phys. Chem.* **1981**, *85*, 3763-3766.

(38) Carra, C.; Iordanova, N.; Hammes-Schiffer, S. Proton-coupled electron transfer in a model for tyrosine oxidation in photosystem II. *J. Am. Chem. Soc.* **2003**, *125*, 10429-10436.

(39) Costentin, C.; Robert, M.; Saveant, J. M. Electrochemical concerted proton and electron transfers. Potential-dependent rate constant, reorganization factors, proton tunneling and isotope effects. *J. Electroanal. Chem.* **2006**, *588*, 197-206.

(40) Gould, I. R.; Farid, S. Specific deuterium isotope effects on the rates of electron transferwithin geminal radical ion pairs. *J. Am. Chem. Soc.* **1988**, *110*, 7883-7885.

(41) Hatcher, E.; Soudackov, A. V.; Hammes-Schiffer, S. Proton-coupled electron transfer in soybean lipoxygenase: Dynamical behavior and temperature dependence of kinetic isotope effects. *J. Am. Chem. Soc.* **2007**, *129*, 187-196.

(42) Hille, R. Electron transfer within xanthine oxidase- A solvent kinetic isotope effect study. *Biochemistry* **1991**, *30*, 8522-8529.

(43) Huynh, M. H. V.; Meyer, T. J.; White, P. S. Proton-coupled electron transfer from nitrogen. A N-H/N-D kinetic isotope effect of 41.4. *J. Am. Chem. Soc.* **1999**, *121*, 4530-4531.

(44) Knapp, M. J.; Rickert, K.; Klinman, J. P. Temperature-dependent isotope effects in soybean lipoxygenase-1: Correlating hydrogen tunneling with protein dynamics. *J. Am. Chem. Soc.* **2002**, *124*, 3865-3874.

(45) Lehnert, N.; Solomon, E. I. Density-functional investigation on the mechanism of H-atom abstraction by lipoxygenase. *J. Biol. Inorg. Chem.* **2003**, *8*, 294-305.

(46) Shafirovich, V.; Dourandin, A.; Luneva, N. P.; Geacintov, N. E. The kinetic deuterium isotope effect as a probe of a proton coupled electron transfer mechanism in the oxidation of guanine by 2-aminopurine radicals. *J. Phys. Chem. B* **2000**, *104*, 137-139.

(47) Sjodin, M.; Styring, S.; Akermark, B.; Sun, L. C. The mechanism for proton-coupled electron transfer from tyrosine in a model complex and comparisons with Y_Z oxidation in photosystem II. *Philos. Trans. R. Soc. London, Ser. B* **2002**, *357*, 1471-1478.

(48) Weatherly, S. C.; Yang, I. V.; Armistead, P. A.; Thorp, H. H. Proton-coupled electron transfer in guanine oxidation: Effects of isotope, solvent, and chemical modification. *J. Phys. Chem. B* **2003**, *107*, 372-378.

(49) Harriman, A. Further comments on the redox potentials of trypthophan and tyrosine. *J. Phys. Chem.* **1987**, *91*, 6102-6104.

(50) Sibert R.; Josowicz, M. P., F.; Veglia, G.; Range, K.; Barry, B.A. Proton-Coupled Electron Transfer in a Biomimetic Peptide as a Model of Enzyme Regulatory Mechanisms. *J. Am. Chem. Soc.* **2007**, *129*, 8.

(51) Magnuson, A.; Berglund, H.; Korall, P.; Hammarstrom, L.; Akermark, B.; Styring, S.; Sun, L. C. Mimicking electron transfer reactions in photosystem II: Synthesis and photochemical characterization of a ruthenium(II) tris(bipyridyl) complex with a covalently linked tyrosine. *J. Am. Chem. Soc.* **1997**, *119*, 10720-10725.

(52) Ahlbrink, R.; Haumann, M.; Cherepanov, D.; Bogershausen, O.; Mulkidjanian, A.; Junge, W. Function of tyrosine Z in water oxidation by photosystem II: Electrostatical potential instead of hydrogen abstractor. *Biochemistry* **1998**, *37*, 1131-1142.

Chapter 3

Proton-Coupled Electron Transfer in Photosystem II: Proton Inventory of a Redox Active Tyrosine

by

David L. Jenson and Bridgette A. Barry

School of Chemistry and Biochemistry and the Parker H. Petit Institute for Bioengineering and Bioscience, Georgia Institute of Technology, Atlanta, Georgia 30332

3.1 Abstract

Photosystem II (PSII) catalyzes the light driven oxidation of water and the reduction of plastoquinone. PSII is a multisubunit membrane protein; the D1 and D2 polypeptides form the heterodimeric core of the PSII complex. Water oxidation occurs at a manganese-containing oxygen evolving complex (OEC). PSII contains two redox active tyrosines, Y_Z and Y_D, which form the neutral tyrosyl radicals, $Y_z^{\bullet}$ and $Y_D^{\bullet}$. Y_D has been assigned as tyrosine 160 in the D2 polypeptide through isotopic labeling and site-directed mutagenesis. While Y_D is not directly involved in the oxidation of water, it has been implicated in the formation and stabilization of the OEC. PSII structures have shown Y_D to be within hydrogen bonding distance of histidine 189 in the D2 polypeptide. Spectroscopic studies have suggested that a proton is transferred between Y_D and histidine 189 when Y_D is oxidized and reduced. In our previous work, we used ^2H_2O solvent exchange to demonstrate that the mechanism of Y_D proton-coupled electron transfer (PCET) differs at high and low pH (Jenson, D. L.; Evans, A.; Barry, B. A. J. Phys. Chem. B 2007, 111, 12599-12604). In this paper, we utilize the proton inventory technique to obtain more information concerning the PCET mechanism at high pH. The hypercurvature of the data provides evidence for the existence of multiple, proton donation pathways to $Y_D^{\bullet}$. In addition, at least one of these pathways must involve the transfer of more than one proton.

3.2 Introduction

Photosystem II (PSII) is a thylakoid membrane bound protein that catalyzes the oxidation of water and the reduction of plastoquinone in a four photon mechanism. Electron transfer is initiated through the photooxidation of a chlorophyll molecule. The electron is transferred to a quinone, Q_A, which acts as a one electron acceptor. Q_A^- reduces Q_B, which can accept two electrons and two protons. Two Q_B molecules are reduced during each catalytic cycle of PSII. This process ultimately results in the production of molecular oxygen from water at a manganese-containing oxygen-evolving complex (OEC). PSII is a multisubunit membrane associated complex. The D1 and D2 polypeptides compose the heterodimeric core of PSII (reviewed in [1]).

Two redox active tyrosines are present in PSII.[2] Y_Z is the oxidant for the OEC and is tyrosine 161 of the D1 polypeptide.[3] Y_D is tyrosine 160 of the D2 polypeptide.[4] Despite their symmetrical arrangement in PSII,[5-8] the function and decay kinetics of $Y_Z^{\bullet}$ and $Y_D^{\bullet}$ are different.[9] $Y_Z^{\bullet}$ decays on the microsecond to millisecond timescale,[10,11] whereas $Y_D^{\bullet}$ decays on the minutes to hours time scale.[2,4] Of the two tyrosines, only Y_Z is directly involved in water oxidation.[3,12,13] However, Y_D may be important in the in the assembly[14] and stability[15] of the OEC. There is a large change in the tyrosine pK_a upon radical formation.[16] Singlet tyrosine has a pK_a of ~10 and the phenolic side chain is expected to be protonated at physiological pH. The tyrosyl radical has a pK_a of < 0 and the phenolic side chain is expected to be deprotonated at physiological pH.[16] This change in phenolic pK_a means that redox-active tyrosines participate in proton-coupled electron transfer (PCET) reactions in enzymes.

Crystal structures, available from 2.9-3.8 Å, indicate that His189 is within hydrogen bonding distance of Y_D.[5-8] Furthermore, EPR and FT-IR spectroscopy have shown that a proton is transferred between Y_D and His189,[17,18] and a one proton rocking mechanism was proposed for this proton-coupled electron transfer reaction.[19] The rocking mechanism is illustrated in Scheme 1. When Y_D is oxidized and the proton is transferred to His189, His189 retains the proton, is cationic, and redonates the proton back to the tyrosyl radical when it is re-reduced (Scheme 1A). Alternatively (Scheme 1B), histidine may lose the proton to another proton acceptor and become neutral after accepting a proton. Scheme 1B requires that a series of proton accepting molecules participate in the PCET reaction. Because protons are transferred along with the electron, kinetic isotope effects may be observable in either the rocking mechanism (Scheme 1A) or the multiproton pathway (Scheme 1B).

Our previous work, utilizing ^2H_2O solvent exchange, has established that a solvent isotope effect is observed on the $Y_D^{\bullet}$ PCET reactions at some pL values, where L is the lyonium ion. This work showed that the mechanism of $Y_D^{\bullet}$ PCET differs at high and low pL.[20] In this paper, we examine the effect of varying ^1H_2O:^2H_2O ratio on the rate of $Y_D^{\bullet}$ reduction at pL 8.0, where a significant solvent isotope effect was observed. This measurement records a proton inventory, which provides insight into the mechanism of proton transfer reactions and into the number of protons transferred in the rate-limiting step of a reaction.[21,22]

Scheme 1

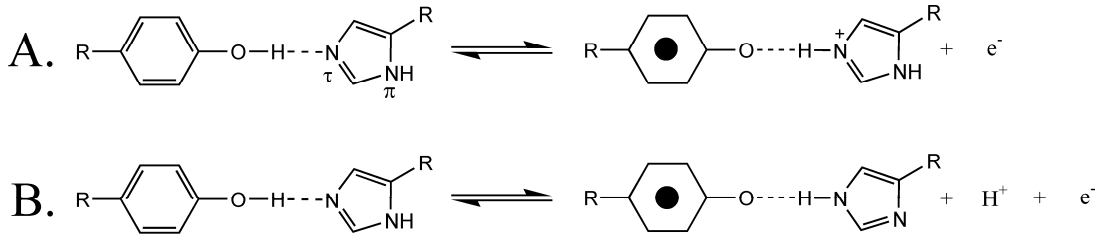

3.3 Materials and Methods

PSII was isolated from market spinach,[23] with the modifications described.[24] Oxygen evolution rates were ≥ 600 μmol O_2 (mg chl h)$^{-1}$.[25] The OEC, as well as the 18-, 24- and 33- kDa polypeptides, were removed from PSII by treatment with tris(hydroxymethyl)aminomethane (Tris) buffer (final concentration 0.8 M Tris-HCl and 2.0 mM tetrasodium ethylenediaminetetraacetic acid (EDTA) at pH 8.0.[26] The pL of the ^2H_2O containing buffers is reported as the uncorrected meter reading, because the small, characteristic solvent isotope effect on the pK_a is approximately offset by the ^2H_2O-induced change in the response of the glass pH electrode.[21] The Tris-treated PSII samples were pooled and dialyzed against SHN buffer (50 mM HEPES, 15 mM NaCl, 400 mM sucrose, pL 8.0) containing varying mole fractions of ^1H_2O: ^2H_2O. The mole fractions (as ^1H_2O:^2H_2O) employed were 100:0, 80:20, 70:30, 60:40, 50:50, 40:60, 30:70 and 0:100 percent. The pL was adjusted using NaO^2H dissolved in L_2O with the appropriate ^1H:^2H mole fraction. ^2H_2O was purchased from Cambridge Isotope Laboratories (99% ^2H_2O enrichment, Andover, CA). The two rounds of dialysis (9 h, followed by 16 h) occurred at 4° C in the dark and utilized dialysis membranes (Spectrum, Laguna Hills, CA) with a 6-8 kDa cutoff. The volume for each round of

dialysis was 500 mL (1:50 dilution). The dialyzed samples were stored at -70° C in 500 μL aliquots until use.

A Bruker EMX X-band electron paramagnetic resonance (EPR) spectrometer equipped with a Bruker ER4119HS cavity was used for EPR analysis.[18,20,27] The cavity was purged with dry nitrogen. The temperature was maintained at 298.1 K using a Bruker ER4131VT variable temperature controller. A Wilmad-Lab Glass (Buena, NJ) WG-808-S-Q small volume flat cell was utilized in all experiments. Chlorophyll concentrations, indicative of $Y_D^{\bullet}$ radical concentration,[28] were determined before the analysis of each sample. The mean chlorophyll concentration of the PSII samples used in the EPR experiments was 1.86 ± 0.15 mg/mL. Because the reduction of the terminal electron acceptor, Q_B, in PSII is associated with proton uptake, all samples contained 10 μM of 3-(3,4-dichlorophenyl)-1,1-dimethylurea (DCMU) to inhibit the formation of Q_B^-. The DCMU was delivered from a stock solution dissolved in ethanol, and the total concentration of ethanol in the samples was < 0.5%. The inhibition of Q_B reduction results in Q_A becoming the terminal electron acceptor. Because the oxidation of Q_A^- is not proton dependent, solvent isotope effects are not expected as a result of Q_A redox chemistry. The microwave power used in these experiments was shown to be non-saturating when compared to a microwave saturation curve[29] obtained under the conditions reported here.

The EPR conditions for kinetic traces were as follows: frequency = 9.46 GHz; static field = 3361 ± 1 G; resolution = 8192 points; microwave power = 1.01 mW; receiver gain = 3.56 x 10^6; modulation frequency = 100 kHz; modulation amplitude = 5.0 G; conversion time = 164 ms; time constant = 5.24 s; analysis time = 1342 s. The PSII

samples were excited by 120 flashes at 1 Hz from a Continuum Surelite III (Santa Clara, CA) Nd:YAG laser at the 532 nm second harmonic. The laser intensity was 50 ± 1 mJ/cm^2. The best fits were to biphasic decay, with one exponential phase giving 89-95% of the amplitude, as determined by the χ^2 values. The laser beam was expanded by using a cylindrical lens in order to give greater coverage over the sample. Kinetic traces were fit using IGOR Pro software (Lake Oswego, OR). Data analysis began 56 s after the cessation of laser excitation in order to eliminate contributions from $Y_Z^{\bullet}$ (τ = 200 ms) and other rapidly decaying radical species.[30] Four sets of kinetics were determined on each individual sample, and the kinetics were found to be comparable within each set. Either six or eight samples were analyzed at each ^1H_2O:^2H_2O mole fraction, for a total of 24 or 32 individual kinetic traces for each point.

A background signal was subtracted from each kinetic transient. Because the decay of $Y_D^{\bullet}$ was not complete between the kinetic traces, due to long half-life of $Y_D^{\bullet}$, an off-resonance scan was taken at a static field, which was -88 G from the field position used to acquire the kinetic transients. This off-resonance scan was taken before each kinetic transient. The off-resonance scan was observed for 336 s, and the mean was subtracted from each point of the following kinetic trace. The EPR conditions for the off-resonance scan were the same as for the kinetic traces, except that the static field was 3273 ± 1 G. At this magnetic field, no free radical resonances were observed.

The EPR conditions for the field swept spectra were as follows: frequency = 9.46 GHz; center field = 3373 G; sweep width = 60 G; resolution = 1024 points; microwave power = 1.01 mW; receiver gain = 3.56 x 10^6; modulation frequency = 100 kHz;

modulation amplitude = 5.0 G; conversion time = 164 ms; time constant = 5.24 s; sweep time = 168 s; sweeps = 6; total time = 1008 s.

3.4 Results and Discussion

Figure 1 shows a typical field swept EPR spectrum of the dark stable radical, $Y_D^{\bullet}$, in a PSII sample. This spectrum was observed one minute following illumination (solid line) and was not detected in a buffer blank (dotted line). The decay rate of $Y_D^{\bullet}$ was monitored after illumination at the indicated field position (Figure 1, arrow and Figure 2). Contributions from $Y_Z^{\bullet}$ and fast decaying radicals were avoided by the fitting procedure (see Materials and Methods). Control experiments showed that the derived kinetics of $Y_D^{\bullet}$ decay were similar when monitored at other field positions (data not shown). Figure 2 shows representative kinetic traces from a single sample, recorded in 100% ^1H_2O (green), a 50:50% ^1H_2O:^2H_2O mixture (red), and 100% ^2H_2O (blue). Fits to the data are shown as superimposed solid lines; the residuals are color-coded in dotted lines at the bottom of the figure. As expected from our previous work, the rate of $Y_D^{\bullet}$ decay slows as the ^2H_2O concentration increases.

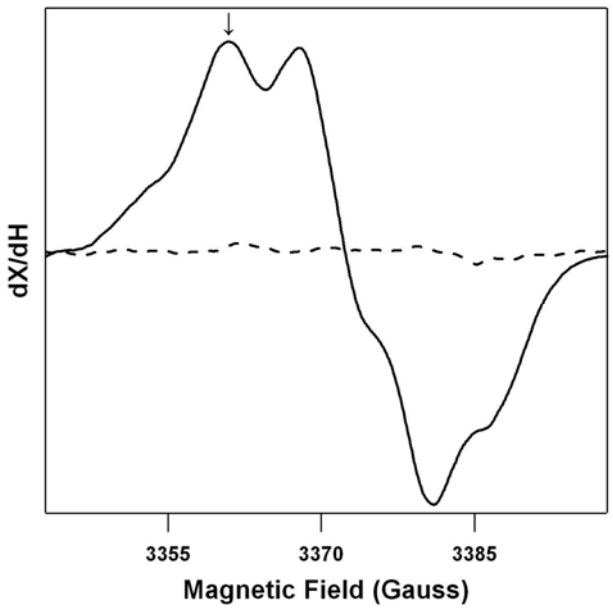

Figure 1. The field swept EPR spectrum of $Y_D^{\bullet}$ in SHN, pH 8.0 buffer (solid line) and a SHN, pH 8.0 buffer blank that lacks the protein sample (dotted line). The arrow indicates the field position at which the kinetic transients were acquired.

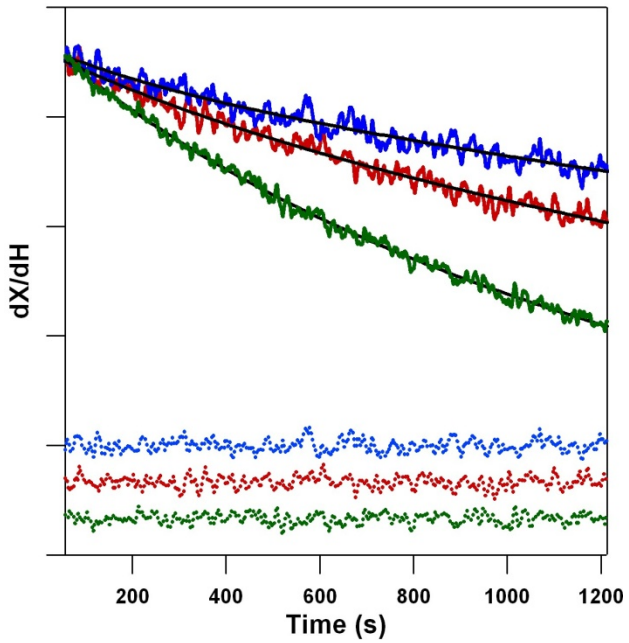

Figure 2. Representative EPR data for kinetic transients (solid lines) and residuals (dotted lines), associated with the decay of $Y_D^{\bullet}$. The data were acquired in 100% ^1H_2O (green), a 50% ^1H_2O:^2H_2O mixture (red), and 100% ^2H_2O (blue). The magnetic field was 3361 ± 1 G. Fits to the data for each ^2H_2O concentration are shown as black lines. Each kinetic trace shown is the average of four traces recorded on one sample. To give the final set of kinetic parameters analyzed in Figure 3, Figure 4 and Table 1, data from 6-8 samples were averaged. For presentation purposes only, the transients shown in this figure were normalized to the data at 100% ^1H_2O. The data for the first 56 s, which were excluded from the fits, are not shown. The tick marks correspond to 10,000 ARB.U. See Materials and Methods for experimental conditions.

Table 1 summarizes the derived rate constants and amplitudes for $Y_D^{\bullet}$ decay at pL 8.0, as a function of ^2H_2O mole fraction. As observed previously, the kinetic fits gave a single majority phase, corresponding to ≥ 89% of the decay amplitude.[20] Additionally, the initial signal amplitude, normalized to chlorophyll concentration, showed no significant variation (Table 1). As expected, the rate of $Y_D^{\bullet}$ decay was slow, occurring over the minutes time scale (Figure 2). The derived rate constants are comparable, within a factor of two, to those derived in our earlier work. However, compared to our previous work at room temperature, the observed, maximum kinetic isotope effect (KIE) in Table

1 is somewhat larger (3.5 ± 0.5 at 25° C versus 2.4 ± 0.5 at 20° C). This is attributed to a temperature effect on the reaction.[31]

Table 1. Rate constants, amplitudes, signal intensity and rates relative to ^2H_2O for $Y_D^{\bullet}$ reduction, as assessed by EPR spectroscopy.[a]

Mole Fraction ^2H_2O	Rate Constant (10^{-4} s^{-1})	Relative Amplitude (%)	EPR Signal Intensity[b] [ARB.U./(mg chl/mL)]	Rate Relative To 100% ^2H_2O
0	5.90 ± 0.43	92 ± 4	22600 ± 1600	3.47 ± 0.55 (KIE)
20	4.10 ± 0.73	91 ± 6	21400 ± 970	2.41 ± 0.55
30	3.35 ± 0.39	89 ± 5	23700 ± 2200	1.97 ± 0.36
40	3.13 ± 0.22	94 ± 1	21600 ± 1700	1.84 ± 0.29
50	2.84 ± 0.56	92 ± 2	21500 ± 2200	1.67 ± 0.40
60	2.23 ± 0.60	91 ± 3	21100 ± 120	1.31 ± 0.40
70	2.57 ± 0.15	94 ± 2	20400 ± 3100	1.51 ± 0.23
100	1.70 ± 0.24	95 ± 3	20300 ± 1600	1.00 ± 0.34

[a]The means are the average of 6-8 samples. The error is reported as ± one standard deviation. All samples contained 10 μM DCMU to inhibit Q_B^- formation. The decay was best fit to a biexponential decay, as determined by χ^2 values. Data were fit using IGOR Pro software (Wavemetrics, Lake Oswego, OR). [b]Signal intensity at 56 s, in arbitrary units.

Figure 3 presents the derived rate constant for $Y_D^{\bullet}$ decay as a function of increasing ^2H_2O mole fraction. Table 2 gives the parameters and equations used to simulate the data in Figures 3 and 4. The data show a nonlinear dependence. This effect is not caused by a limitation of ^2H exchange. Previous studies have shown that the exchange of the Y_D phenoxyl proton occurs with a half-life of approximately 9 h at pL 7.0.[32] Given that the conditions employed here utilize higher pL (8.0), our total dialysis time of 25 h should be sufficient for complete ^2H exchange in the Y_D pocket.

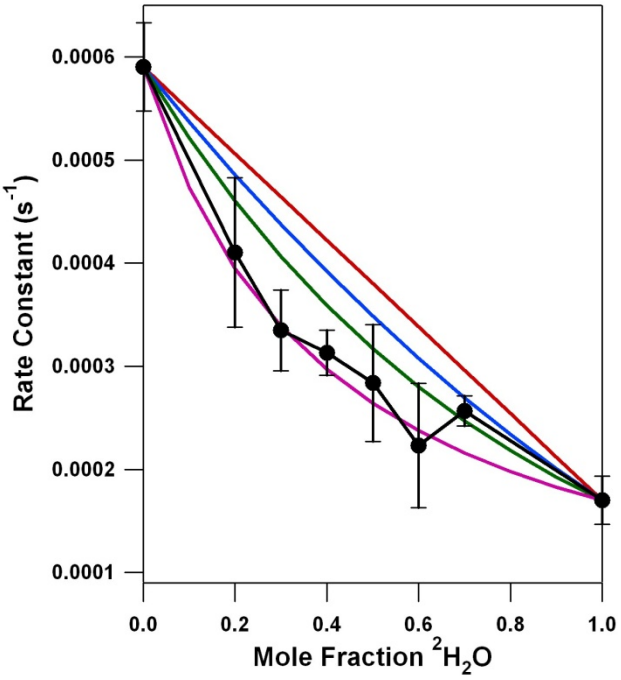

Figure 3. Proton inventory for the $Y_D^{\bullet}$ PCET reaction at pL 8.0. The black line is the experimental data, showing the dependence of rate constant on mole fraction $^2H^2O$, as assessed by transient EPR spectroscopy. The kinetic parameters are shown in Table 1. The error bars represent one standard deviation. The red line simulates a one proton, transition state proton inventory. The blue line simulates a two proton, transition state proton inventory. The green line simulates a "many proton" inventory. The pink line, an example of hypercurvature, simulates a one proton, reactant state proton inventory. See Table 2 for the parameters and equations employed to simulate the proton inventory data.

For comparison with the data, Figure 3 shows simulations, illustrating the expected plots for a one (red), two (blue), and "many proton" (green) transfer in the transition state.[21,22] The relation between rates, fractionation factors and the mole fraction deuterium in the solvent is given by the Gross-Butler equation,

$$v_n = v_0 * \frac{\prod_i (1 - n + n\phi_{Ti})}{\prod_j (1 - n + n\phi_{Rj})}$$

where n is the mole fraction of ^2H_2O; v_n is the rate constant at mole fraction n; v_0 is the rate constant in pure ^1H_2O; the products, *i* and *j*, are over the number of protons

transferred in the transition and reactant state, respectively; ϕ_R is the transition state fractionation factor; and ϕ_R is the reaction state fractionation factor. Fractionation factors measure the preference of a particular site for deuterium relative to a bulk water molecule.[21,22] The kinetic isotope effect (KIE) is defined as KIE = $k_H/k_D = \phi_R/\phi_R$, where k_D is the rate constant in ^2H_2O and k_H is the rate constant in ^1H_2O. If it is assumed that the reactant state fractionation factor is equal to one, the denominator in the Gross-Butler equation reduces to unity and only the numerator remains.[21,22] This assumption is usually valid in proteins, as most protonic sites in proteins (including carboxylic acid, imidazole, amine and hydroxyl functional groups) have reactant state fractionation factors that are nearly identical to unity.[21,22] The sulfhydyl group is known to have a reactant state fractionation factor that is not near unity (ϕ_R = 0.55), but we do not expect proton donation from cysteine in our proton inventory experiments.[5-8]

Table 2. Parameters and equations used to generate simulated data in Figure 3 and Figure 4.

Plot Type	v_0	v_{100}	ϕ_{T_1}	ϕ_{T_2}	ϕ_R	Equation*
One Proton[a]	0.000590	0.000170	0.288	NA	1.00	$v_n = v_0 * (1 - n + 0.288n)$
Two Proton[a]	0.000590	0.000170	0.288	NA	1.00	$v_n = v_0 * (1 - n + n\sqrt{0.288})^2$
Many Proton[a]	0.000590	0.000170	0.288	NA	1.00	$v_n = v_0 * (0.288)^n$
Reactant State[a] (Hypercurvature)	0.000590	0.000170	1.00	NA	3.47	$v_n = v_0 * (1 - n + 3.47n)^{-1}$
Multipathway[b] (Hypercurvature)	0.000590	0.000170	0.083	0.97	1.00	$v_n = v_0 * [0.75 * (0.083)^n + 0.25 * (1 - n + 0.97n)]$

*The relation between rates, fractionation factors and the mole fraction deuterium in the solvent is given by the Gross-Butler equation,

$$v_n = v_0 * \frac{\prod_i (1 - n + n\phi_{Ti})}{\prod_j (1 - n + n\phi_{Rj})}$$

where n is the mole fraction of ^2H_2O; v_n is the rate constant at mole fraction n; v_0 is the rate constant in pure ^1H_2O; the products, *i* and *j*, are over the number of protons transferred in the transition and reactant state, respectively; ϕ_T is the transition state fractionation factor; and ϕ_R is the reaction state fraction factor. The kinetic isotope effect (KIE) is defined as KIE = $k_H/k_D = \phi_R/\phi_T$, where k_D is the rate constant in ^2H_2O and k_H is the rate constant in ^1H_2O. In the multipathway model, 0.75 represents the fractional contribution to the rate from ϕ_{T_1} and 0.25 represents the fractional contribution to the rate from ϕ_{T_2}. [a]Data simulated in Figure 3. [b]Data simulated in Figure 4.

The proton inventory technique monitors the number of protons transferred in the rate-limiting step of an enzymatic reaction.[22] When the reactant state fractionation factor ϕ_R is one and the denominator of the Gross-Butler equation is unity, the equation predicts a linear proton inventory if one proton is transferred (Figure 3, red line; and Table 2). For example, many serine proteases exhibit one proton, transition state proton inventories,[22,33] due to the abstraction of a single serine proton by imidazole during the rate-limiting step.[22] A linear proton inventory would be expected in the rocking model for Y_D/His189D2 PCET (Scheme 1A). In this case, the KIE would be expected to be generated through a single proton transfer in the transition state.[22]

On the other hand, a quadratic dependence in a proton inventory experiment indicates that two protons are being transferred in the rate-limiting step (Figure 3, blue line; and Table 2). Generally, the individual values of ϕ_T are not known and $(1/KIE)^{1/2}$ is assigned as an average value.[21,22] For example, ribonuclease A gives a two proton, transition state proton inventory.[34] The rate-limiting, concerted transfer occurs when the phosphodiester bond is cleaved by the donation of a proton from histidine and the abstraction of the second proton from water.[34]

A proton inventory experiment normally lacks the resolution to differentiate between mechanisms transferring more than two protons in the rate-limiting step.[22] Curves of cubic and higher order are usually separated by an amount less than the error in measurement.[22] As a consequence, when more than two protons are transferred in the rate-limiting step, the mechanism is described as "many proton" and an exponential dependence is observed (Figure 3, green line).[21,22] This model is the limiting case of the Gross-Butler equation, as the number of protons transferred becomes large.[22] Again, the individual values of ϕ_T are not usually known and 1/KIE is taken as the average fractionation factor.[21,22] An example of this type of proton inventory occurs in carbonic anhydrase,[35] in which a coordinated zinc ion transfers a proton to a histidine via a water transport chain.[35]

The interpretations described above apply if the reactant state fractionation factors are equal to unity (i.e., the kinetic isotope effect is generated in the transition state) and if one step in the reaction is rate-limiting.[36] If these conditions are not met, more complex interpretations are required. One such example occurs with proton inventory plots that exhibit hypercurvature (Figure 3, pink line and Figure 4), that is, that are bowed more

deeply then the many proton, exponential plot (Figure 3, green line).[22] Figures 3 and 4 show that hypercurvature is observed in our proton inventory data. This hypercurvature indicates that PCET to $Y_D^{\bullet}$ must be more complex than the one proton rocking mechanism (Scheme 1A).

The data were fit well with two different models. In the first, the KIE is solely attributable to one proton being transferred in the reactant state, when the transition state fractionation factor is equal to unity (Figure 3, pink line). In the second, there is more than one proton donor to $Y_D^{\bullet}$, this is known as a multipathway model (Figure 4). The parameters used to fit both the one proton, reactant state model and the multipathway model are shown in Table 2. Scatter plots of the theoretical rate constant versus the experimental rate constant for each model were constructed (data not shown). The one proton, reactant state model gave a correlation coefficient of 0.991, a slope of 1.01 and a y-intercept of 0.000. The multipathway model gave a correlation coefficient of 0.990, a slope of 0.999 and a y-intercept of 0.000. Therefore, the fits to each model are highly correlated with the experimental data. The implications are discussed below.

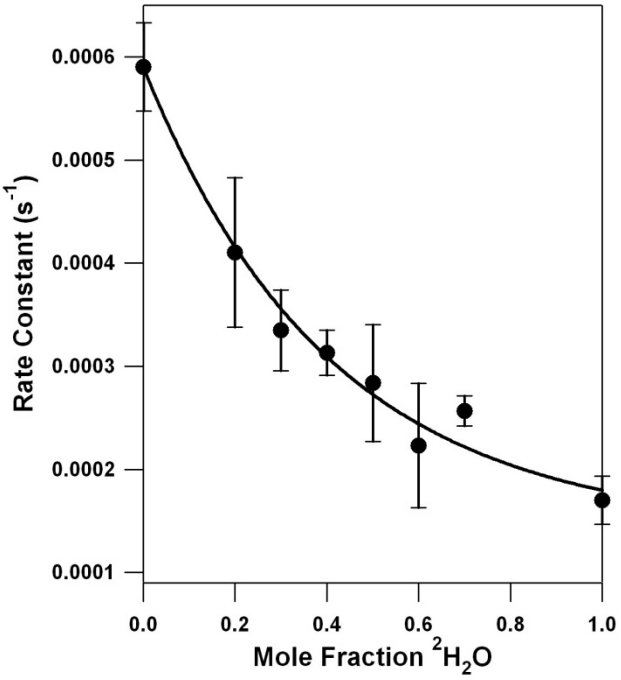

Figure 4. Simulation of a multipathway proton inventory for $Y_D^{\bullet}$. The experimental data are shown as black dots. The error bars represent one standard deviation. The black line simulates a multipathway fit to the data. See Table 2 for the parameters and equations employed to simulate the proton inventory data.

A proton inventory experiment will exhibit hypercurvature under two possible scenarios. The first explanation for hypercurvature occurs when the KIE results from reactant state fractionation factor for one or more reactant state protons.[22] A model with a significant reaction state fractionation factor fit to our data (Figure 3, pink line and Table 2). However, if the mechanism is to be assigned solely to reactant state fractionation factors, then the magnitude of the required fractionation factors must be reasonable. To explain our data, ϕ_R must be at least 3.47 (Tables 1 and 2) if a single reactant state proton is transferred in the rate-limiting step. ϕ_R must be at least $(3.47)^{1/2}$ = 1.86 if two reactant state protons transferred in the rate-limiting step. These ϕ_R values are too large to be realistic, because reactant state fractionation factors are in the range of

0.4-1.3 and are usually assumed to be unity.[37] Additionally, there are only a few instances in which reaction state fractionation factors have been reported in enzymes and rarely is the value >1.[37] Significant reactant state fractionation factors in enzymes usually occur through interactions with cysteine (ϕ_R = 0.55), metal-bound waters (ϕ_R = 0.4-0.8), and hydronium (ϕ_R = 0.69).[37] Given the magnitude of the KIE observed in our experiments (Table 1), we conclude that the hypercurvature observed in our data is unlikely to occur as a result of reactant state fractionation factors.

The second possible explanation for hypercurvature is the existence of multiple proton donation pathways.[22] For example, in a system in which there are two parallel pathways for proton transfer (Figure 5), k_{obs} is the sum of the two rate constants, $k_1 + k_2$. Substituting in the Gross-Butler equation, assuming the reactant state fractionation factors are unity and accounting for the relative contribution of k_1 and k_2 in k_{obs} the following can be derived:

$$v_n = v_0 * [f_1 * \prod_i (1 - n + n\phi_{Ti}) + (1 - f_1) * \prod_j (1 - n + n\phi_{Tj})]$$

where f_1 equals the fractional contribution towards k_{obs} from k_1 and $(1-f_1)$ equals the fractional contribution towards k_{obs} from k_2. It is important to note that if both parallel pathways involve only one proton, then only a linear proton inventory will result, because the sum of two lines gives a linear slope.

The literature provides evidence of a proton donor to $Y_D^{\bullet}$ other than His189D2. In a His189Leu site-directed mutant, an EPR signal attributable to $Y_D^{\bullet}$ was detected, and the decay of this signal showed the unusually slow reduction kinetics of $Y_D^{\bullet}$.[18] The yield of $Y_D^{\bullet}$ was increased, and its decay rate was accelerated to a value similar to that seen in the wild-type upon addition of imidazole into the medium.[18] The indication is that

imidazole influences the rate of $Y_D^{\bullet}$ reduction, potentially by acting as a proton donor.[18] It has also been demonstrated that $Y_D^{\bullet}$ is able to form in His189Gln mutants.[38] In that work, the observed value of the g_x component of 2.00832 indicated that $Y_D^{\bullet}$ was neutral,[38] as opposed to the low g_x component value (< 2.0045) that would be expected for a phenoxyl radical cation.[39,40] The observation of a neutral tyrosyl radical in the His189Gln mutant indicates the presence of a proton acceptor other than His189D2. It is clear from these two experiments that $Y_D^{\bullet}$ is able to form in the absence of His189 and a secondary proton acceptor is also active in the $Y_D^{\bullet}$ PCET mechanism.

As shown in Figure 4, a multiproton, parallel transfer pathway can provide a good fit to the experimental data. However, while the set of parameters shown in Table 2 adequately represent the data, our fitting procedure does not establish that this combination of parameters is a unique solution. In Figure 4, the first proton donation pathway is modeled as a "many proton" pathway in 75% abundance with a transition state fractionation factor of 0.083 (Table 2). The exact number of protons transferred cannot be determined in a "many proton" model. We can only determine that the number of protons being transferred is greater than three. Considering a model involving three protons, the composite fractionation factor of 0.083 is equivalent to three protons that each have a fractionation factor of $(0.083)^{1/3} = 0.44$. This is a reasonable value in biological systems, as a fraction factor of 0.44 is equivalent to a kinetic isotope effect of 2.3. Models consisting of more than three protons also result in reasonable fractionation factors. A four proton model would produce four equivalent fractionation factors of $(0.083)^{1/4} = 0.54$ (KIE = 1.9); whereas, a five proton model would produce five equivalent fractionation factors of $(0.083)^{1/5} = 0.61$ (KIE = 1.6). In the limiting case, as

the number of protons transferred grows large (as in the case of solvent effects), fractionation factors asymptote at unity in the "infinite site" model. The second proton donation pathway is modeled as a one proton, transition state pathway in 25% abundance (Table 2). This pathway is modeled as having a small transition state fractionation factor of 0.97. We have modeled the multiproton pathway as occurring through either His189D2 (Figure 5A) or through a chain of water molecules (Figure 5B). The rational for these assignments and their implications are discussed below.

In Figure 5, the His189 protonation pathway is shown as reaction 1. The pathway involving His189D2 may be either a multiproton (Figure 5A) or a one proton (Figure 5B) pathway. In proteins, histidine typically has a pK_a value of approximately 6.0. Therefore, in our experiments at pL 8.0, histidine should be in the neutral form when Y_D is in the reduced, singlet state (Figure 5A). When Y_D is oxidized, the histidine will accept a proton from tyrosine, forming a histidine cation and giving a one proton pathway (Scheme 1A). If the histidine cation does deprotonate to another proton acceptor, then a neutral imidazole and a multiproton pathway will result (Scheme 1B).

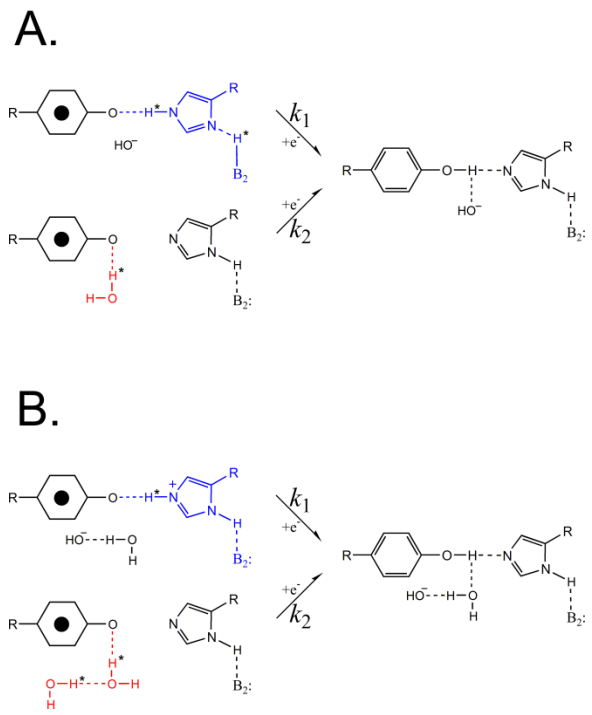

Figure 5. Schematic of proton donation pathways for $Y_D^{\bullet}$. The asterisks indicate the protons in motion. **A.** In pathway 1, histidine (blue) is involved in the multiproton pathway. In pathway 2, a water molecule (red) is proposed to act as a single proton donor. **B.** In pathway 1, histidine (blue) is proposed to act as a single proton donor. In pathway 2, a chain of water molecules (red) are involved in the multiproton pathway.

Given the pK_a of histidine, a neutral His189D2 would be expected at pL 8.0 and, by extension, the histidine should deprotonate (presumably to a secondary proton acceptor) upon Y_D oxidation. This view is supported by the literature.[39-43] For example, it was reported that the value of the $Y_D^{\bullet}$ g_x component was 2.00643 when generated cryogenically at alkaline pH, as opposed to the reported value of 2.00756 when the radical was generated at physiological temperature.[41] This lower g_x component is indicative of an electropositive environment near $Y_D^{\bullet}$, such as an imidazolium cation.[39-41,44] With warming, the g_x component shifted from 2.00643 to 2.00756. One explanation

for this thermal g_x component shift is a relaxation of the protein and the subsequent deprotonation of the imidazolium to form the neutral imidazole.[41]

If the His189D2 proton transfer pathway is multiproton, the identity of the second proton acceptor is of interest. PSII crystal structures (Figure 6) indicate that Arg294D2 is 2.8 ± 0.4 Å from the π-nitrogen of His189D2 and may be able to act as a proton acceptor from His189D2.[5-8] However, the arginine must be deprotonated to accept a proton from His189, and this would require a pK_a shift of 4-5 orders of magnitude. This change in pK_a may be unlikely, but could possibly be achieved as a result of the relatively hydrophobic nature of the Y_D pocket[5-8] or as a result of electrostatic interactions near Arg294. Further reinforcing the importance of Arg294D2, a Arg294Trp mutant was shown to be unable to grow photoautotrophically and was quickly deactivated by light.[45] However, the reason for the mutant's inability to grow photoautotrophically may be structural,[45] because Arg294D2 sits at the interface of the D2 and CP47 subunits and is presumed to be within hydrogen bonding distance of Glu364CP47.[5-8]

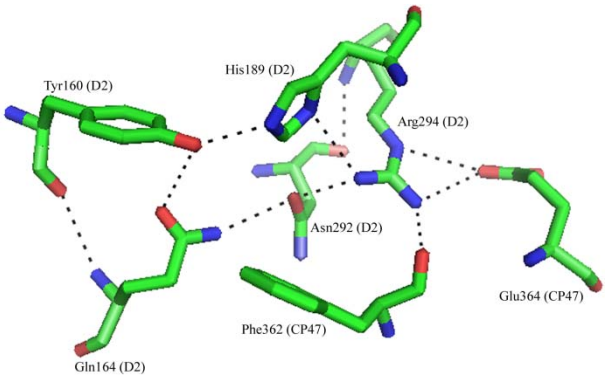

Figure 6. X-ray structure of PSII at 3.0 Å showing the local environment of Y_D (pdb entry 2AXT[5]).

If the His189D2 pathway were to involve only a single proton, then the competing pathway must involve multiple protons (Figure 5B). The proton accepting groups on the second parallel pathway could be bound water molecules (Figure 5B, reaction 2), because the Y_D pocket has been shown to be accessible to the surrounding media. For example, it was reported that at least two water molecules are structurally coupled to Y_D, either through a direct hydrogen bond or within the hydrogen bond network around Y_D (Figure 6).[46] However, it should be noted that the environment of $Y_D^{\bullet}$ can be altered by ionic interactions.[47] Second, an exchangeable proton that is hydrogen bonded to the phenolic oxygen of $Y_D^{\bullet}$ has been detected.[32,48] Finally, it is has been demonstrated that imidazole can be exchanged into the region surrounding Y_D in a site-directed mutant.[18]

It is possible that the "many proton" model we observe in these experiments is the result of solvent effects.[22,35] Solvent effects occur when there is a change in conformation or charge distribution over the course of the reaction that alters the fractionation factors of many of the solvating water molecules.[22,35] Each of these individual sites has a very small change in its fractionation factor, but the effect is collectively large. The overall result is also a "many proton" inventory.[22,35] We cannot eliminate the possibility that a solvent effect is occurring; however, there is sufficient evidence to support a multiproton pathway consisting of either His189D2 or a chain of water molecules.

In conclusion, we present data that show that $Y_D^{\bullet}$ PCET is more complex than previously suggested, at least at high pH values. To explain our data, multiple PCET pathways must exist at pL 8.0. Also, at least one of these pathways must be "many proton" and involve sequential proton transfer reactions. We propose that one PCET

pathway involves His189D2, which may act as a proton relay, and that the second PCET pathway involves water as a proton donor.

3.5 Acknowledgment.

This work was supported by the National Institutes of Health, GM43273 (B. A. B.).

3.6 References

(1) Nelson, N.; Yocum, C. F. Structure and function of photosystems I and II. *Annu. Rev. Plant Biol.* **2006**, *57*, 521-565.

(2) Barry, B. A.; Babcock, G. T. Tyrosine radicals are involved in the photosynthetic oxygen-evolving system. *Proc. Natl. Acad. Sci. USA* **1987**, *84*, 7099-7103.

(3) Debus, R. J.; Barry, B. A.; Sithole, I.; Babcock, G. T.; McIntosh, L. Directed mutagenesis indicates that the donor to P_{680}^{+} in photosystem II is Tyr-161 of the D1 polypeptide. *Biochemistry* **1988**, *27*, 9071-9074.

(4) Debus, R. J.; Barry, B. A.; Babcock, G. T.; McIntosh, L. Site-specific mutagenesis identifies a tyrosine radical involved in the photosynthetic oxygen-evolving complex. *Proc. Natl. Acad. Sci. USA* **1988**, *85*, 427-430.

(5) Loll, B.; Kern, J.; Saenger, W.; Zouni, A.; Biesiadka, J. Towards complete cofactor arrangement in the 3.0 Å resolution structure of photosystem II. *Nature* **2005**, *438*, 1040-1044.

(6) Ferreira, K. N.; Iverson, T. M.; Maghlaoui, K.; Barber, J.; Iwata, S. Architecture of the photosynthetic oxygen-evolving center. *Science* **2004**, *303*, 1831-1837.

(7) Biesiadka, J.; Loll, B.; Kern, J.; Irrgang, K.-D.; Zouni, A. Crystal structure of cyanobacterial photosystem II at 3.2 Å resolution: a closer look at the Mn-cluster. *Phys. Chem. Chem. Phys.* **2004**, *20*, 4733-4736.

(8) Guskov, A.; Kern, J.; Gabdulkhakov, A.; Broser, M.; Zouni, A.; Saenger, W. Cyanobacterial photosystem II at 2.9- Å resolution and the role of quinones, lipids, channels and chloride. *Nat. Struct. Mol. Biol.* **2009**, *16*, 334-342.

(9) Rutherford, A. W.; Boussac, A.; Faller, P. The stable tyrosyl radical in Photosystem II: why D? *Biochim. Biophys. Acta* **2004**, *1655*, 222-230.

(10) Babcock, G. T.; Blankenship, R. E.; Sauer, K. Reaction kinetics for positive charge accumulation on the water side of chloroplast Photosystem II. *FEBS Lett.* **1976**, *61*, 286-289.

(11) Dekker, J. P.; Gorkom, H. J. V.; Brok, M.; Ouwehand, L. Optical characterization of photosystem II electron donors. *Biochim. Biophys. Acta* **1984**, *764*, 301-309.

(12) Gerken, S.; Brettel, K.; Schlodder, E.; Witt, H. T. Optical characterization of the immediate donor to Chlorophyll a_{II}^{+} in O_2-evolving photosystem II complexes. *FEBS Lett.* **1988**, *237*, 69-75.

(13) Boerner, R. J.; Barry, B. A. Isotopic labeling and EPR spectroscopy show that a tyrosine residue is the terminal electron donor, Z, in manganese-depleted photosystem II preparations. *J. Biol. Chem.* **1993**, *268*, 17151-17154.

(14) Ananyev, G. M.; Sakiyan, I.; Diner, B. A.; Dismukes, G. C. A functional role for tyrosine-D in assembly of the inorganic core of the water complex of photosystem II and the kinetics of water oxidation. *Biochemistry* **2002**, *41*, 974-980.

(15) Styring, S.; Rutherford, A. W. In the oxygen-evolving complex of photosystem II the S_0 state is oxidized to the S_1 State by D^{+} (Signal II_{slow}). *Biochemistry* **1987**, *26*, 2401-2405.

(16) Dixon, W. T.; Murphy, D. Determination of the acidity constants of some phenol radical cations by means of electron spin resonance. *J. Chem. Soc. London, Faraday Trans. II* **1976**, *72*, 1221-1229.

(17) Campbell, K. A.; Peloquin, J. M.; Diner, B. A.; Tang, X.-S.; Chisholm, D. A.; Britt, R. D. The τ-Nitrogen of D2 histidine 189 is the hydrogen bond donor to the tyrosine radical $Y_D^{\bullet}$ of photosystem II. *J. Am. Chem. Soc.* **1997**, *119*, 4787-4788.

(18) Kim, S.; Liang, J.; Barry, B. A. Chemical complementation identifies a proton acceptor for redox-active tyrosine D in photosystem II. *Proc. Natl. Acad. Sci. USA* **1997**, *94*, 14406-14412.

(19) Babcock, G. T.; Barry, B. A.; Debus, R. J.; Hoganson, C. W.; Atamian, M.; McIntosh, L.; Sithole, I.; Yocum, C. F. Water oxidation in photosystem II: From radical chemistry to multielectron chemistry. *Biochemistry* **1989**, *28*, 9557-9565.

(20) Jenson, D. L.; Evans, A.; Barry, B. A. Proton-coupled electron transfer and tyrosine D of photosystem II. *J. Phys. Chem. B* **2007**, *111*, 12599-12604.

(21) Schowen, K. B.; Schowen, R. L. Solvent isotope effects of enzyme systems. *Methods Enzymol.* **1982**, *87*, 551-606.

(22) Venkatasubban, K. S.; Schowen, R. L. The proton inventory technique. *CRC Crit. Rev. Biochem.* **1984**, *17*, 1-44.

(23) Berthold, D. A.; Babcock, G. T.; Yocum, C. F. A highly resolved, oxygen-evolving Photosystem II preparation from spinach thylakoid membranes. *FEBS Lett.* **1981**, *134*, 231-234.

(24) Anderson, L. B.; Ouellette, A. J. A.; Barry, B. A. Probing the primary structure of photosystem II with amines and phenylhydrazine. *J. Biol. Chem.* **2000**, *275*, 4920-4927.

(25) Barry, B. A. Tyrosyl radicals in photosystem II. *Methods Enzymol.* **1995**, *258*, 303-319.

(26) Yamomoto, Y.; Doi, M.; Tamura, N.; Nishimura, N. Release of polypeptides from highly active O_2-evolving photosystem-2 preparation by Tris treatment. *FEBS Lett.* **1981**, *133*, 265-268.

(27) Kim, S.; Ayala, I.; Steenhuis, J. J.; Gonzalez, E. T.; Razeghifard, M. R.; Barry, B. A. Infrared spectroscopic identification of the C-O stretching vibration associated with the tyrosyl $Z^{\bullet}$ and $D^{\bullet}$ radicals in photosystem II. *Biochim. Biophys. Acta* **1998**, *1366*, 330-354.

(28) Patzlaff, J. S.; Barry, B. A. Pigment quantitation and analysis by HPLC reverse phase chromatography: A characterization of antenna size in oxgyen-evolving photosystem II preparations from cyanobacteria and plants. *Biochemistry* **1996**, *35*, 7802-7811.

(29) Poole, C. P. *Electron Spin Resonance: A Comprehensive Treatise on Experimental Techniques*; Dover Publications: Mineola, N.Y., 1996.

(30) Ma, C.; Barry, B. A. Electron paramagnetic resonance characterization of tyrosine radical, M^{+}, in site-directed mutants of photosystem II. *Biophys. J.* **1996**, *71*, 1961-1972.

(31) Edwards, S. J.; Soudackov, A. V.; Hammes-Schiffer, S. Analysis of Kinetic Isotope Effects for Proton-Coupled Electron Transfer Reactions. *J. Phys. Chem. A* **2009**, *113*, 2117-2126.

(32) Diner, B. A.; Force, D. A.; Randall, D. W.; Britt, R. D. Hydrogen bonding, solvent exchange, and coupled proton and electron transfer in the oxidation and reduction of redox-active tyrosine Y_Z in Mn-depleted core complexes of photosystem II. *Biochemistry* **1998**, *37*, 17931-17943.

(33) Elrod, J. P.; Hogg, J. L.; Quinn, D. M.; Venkatasubban, K. S.; Schowen, R. L. Protonic reorganization and substrate structure in catalysis by serine proteases. *J. Am. Chem. Soc.* **1980**, *102*, 3917-3922.

(34) Matta, M. S.; Vo, D. T. Proton inventory of the 2nd step of ribonuclease catalysis. *J. Am. Chem. Soc.* **1986**, *108*, 5316-5318.

(35) Venkatasubban, K. S.; Silverman, D. N. Carbon dioxide hydration activity of carbonic anhydrase in mixtures of water and deuterium hydroxide. *Biochemistry* **1980**, *19*, 4984-4989.

(36) Alvarez, F. J.; Ermer, J.; Hubner, G.; Schellenberger, A.; Schowen, R. L. The linkage of catalysis and regulation in enzyme action, solvent isotope effects as probes of protonic sites in the yeast pyruvate decarboxylase mechanism. *J. Am. Chem. Soc.* **1995**, *117*, 1678-1683.

(37) Quinn, D. M.; Sutton, L. D.; Cook, P. F., Ed.; CRC Press, Inc.: Boca Raton, FL, 1991, pp 73-126.

(38) Un, S.; Tang, X.-S.; Diner, B. A. 245 GHz High-field EPR study of tyrosine-$D^{\bullet}$ and Tyrosine-$Z^{\bullet}$ in mutants of photosystem II. *Biochemistry* **1996**, *35*, 679-684.

(39) Brynda, M.; Britt, R. D. Density Functional Theory calculations on the magnetic properties of the model tyrosine radical-histidine complex mimicking tyrosyl radical $Y_D^{\bullet}$ in Photosystem II. *Res. Chem. Intermed.* **2007**, *33*, 863-883.

(40) Benisvy, L.; Bittl, R.; Bothe, E.; Garner, C. D.; McMaster, J.; Ross, S.; Teutloff, C.; Neese, F. Phenoxyl radicals hydrogen-bonded to imidazolium: Analogues of tyrosyl D of photosystem II: High-field EPR and DFT studies. *Angew. Chem.* **2005**, *44*, 5314-5317.

(41) Faller, P.; Goussias, C.; Rutherford, A. W.; Un, S. Resolving intermediates in biological proton-coupled electron transfer: A tyrosyl radical prior to proton movement. *Proc. Natl. Acad. Sci. USA* **2003**, *100*, 8732-8735.

(42) Un, S.; Atta, M.; Fontecave, M.; Rutherford, A. W. g-Values as a probe of the local protein environment: High-field EPR of tyrosyl radicals in ribonucleotide reductase and photosystem II *J. Am. Chem. Soc.* **1995**, *117*, 10713-10719.

(43) Engstrom, M.; Himo, F.; Graslund, A.; Minaev, B.; Vahtras, O.; Agren, H. Hydrogen bonding to tyrosyl radical analyzed by ab initio g-tensor calculations. *J. Phys. Chem. A* **2000**, *104*, 5149-5133.

(44) Maniero, A. L.; Chis, V.; Zoleo, A.; Brustolon, M.; Mezzetti, A. Three different tyrosyl radicals identified in L-tyrosine HCl crystals upon gamma-irradiation: Magnetic characterization and temporal evolution. *J. Phys. Chem. B* **2008**, *112*, 3812-3820.

(45) Ermakova-Gerdes, S.; Yu, Z.; Vermaas, W. Targeted random mutagenesis to identify functionally important residues in the D2 protein of photosystem II in *Synechocystis sp.* strain PCC 6803. *J. Bacteriol.* **2001**, *183*, 145-154.

(46) Takahashi, R.; Sugiura, M.; Noguchi, T. Water molecules coupled to the redox-active tyrosine Y_D in photosystem II as detected by FTIR Spectroscopy. *Biochemistry* **2007**, *46*, 14245-14249.

(47) Kim, S.; Barry, B. A. Vibrational spectrum associated with the reduction of tyrosyl radical $D^{\bullet}$ in photosystem II: a comparative biochemical and kinetic study. *Biochemistry* **1998**, *37*, 13882-13892.

(48) Force, D. A.; Randall, D. W.; Britt, R. D.; Tang, X.-S.; Diner, B. A. ^2H ESE-ENDOR study of hydrogen bonding to the tyrosine radicals $Y_D^{\bullet}$ and $Y_Z^{\bullet}$ of photosystem II. *J. Am. Chem. Soc.* **1995**, *117*, 12643-12644.

Chapter 4

Hydrogen Bonding States of Redox Active Tyrosine Radicals in Photosystem II

by

David L. Jenson,[1] Oleg G. Poluektov,[2] Lisa M. Utschig[2] and Bridgette A. Barry[1]

[1]School of Chemistry and Biochemistry and the Parker H. Petit Institute for Bioengineering and Bioscience, Georgia Institute of Technology, Atlanta, Georgia 30332

[2]Chemical Sciences and Engineering Division, Argonne National Laboratory, 9700 South Cass Avenue, Argonne Illinois, 60439

4.1 Abstract

Photosystem II is a light activated enzyme containing two redox active tyrosine residues. The first, $Y_D^{\bullet}$, is tyrosine 160 in the D2 polypeptide. The second, $Y_Z^{\bullet}$, is tyrosine 161 in the D1 polypeptide. Despite their pseudo-C_2 symmetry, these tyrosine residues have different redox properties. Both tyrosines have a histidine within hydrogen bonding distance. Y_D is within hydrogen bonding distance of His189D2. The histidine is able to accept a proton when Y_D is oxidized in a proton-coupled electron transfer (PCET) reaction. In our previous work (Chapter 3), we have identified another proton donor to $Y_D^{\bullet}$, but it is not known if this alternate donor is directly involved in a hydrogen bond with the radical. In order to elucidate the PCET reduction mechanism for $Y_D^{\bullet}$ and to understand how the environment surrounding these tyrosines may alter their redox chemistries, we have examined the $Y_D^{\bullet}$ and $Y_Z^{\bullet}$ EPR spectrum at 130 GHz as a function of pH. The analysis of the g-tensor components suggest that both tyrosyl radicals are likely hydrogen bonded to neutral species. Additionally, the environment surrounding one tyrosyl radical, $Y_Z^{\bullet}$, exhibits significant changes as a function of pH. This dependence on pH for the $Y_Z^{\bullet}$ g_x component is attributed to an increasingly electropositive environment as the pH becomes more alkaline, most likely due to a change in hydrogen bond strength or to additional hydrogen bond donors. In contrast, the data suggest that the environment surrounding the second tyrosyl radical, $Y_D^{\bullet}$, changes little throughout the pH range examined. For $Y_D^{\bullet}$, the implication is that His189 may accept a proton from Y_D during oxidation and then deprotonate from its π-nitrogen to form the neutral His189. This finding is in agreement with the previous determination that multiple protons are transferred in the rate-limiting step of $Y_D^{\bullet}$ reduction.

4.2 Introduction

Photosystem II has two redox active tyrosine residues that are arranged in pseudo-C_2 symmetry.[1-4] The first, Y_D, is tyrosine 160 of the D2 polypeptide.[5] The second, Y_Z, is tyrosine 161 of the D1 polypeptide.[6] Both tyrosines have a histidine residue within hydrogen bonding distance; His189D2 in the case of Y_D, and His190D1 in the case of Y_Z.[1-4] It has been proposed that both tyrosines deprotonate to their respective histidine residues upon oxidation and accept a proton from histidine upon reduction in a proton-coupled electron transfer (PCET) mechanism.[7] Through ^2H and ^{15}N ESE-ENDOR spectroscopy, His189D2 has been shown to have an exchangeable hydrogen bond to $Y_D^{\bullet}$.[8,9] In contrast, $Y_Z^{\bullet}$ is believed to be in a more disordered environment.[9-11]

The protonation state of histidine is important factor in examining the mechanisms of tyrosine redox chemistry in PSII. There is not currently a consensus in the literature concerning the protonation state of histidine for either of the oxidized tyrosines. It has been proposed that a rocking mechanism occurs through two possible mechanisms (Scheme 1 and Figure 1).[7] The first is a transfer of a proton to histidine upon tyrosine oxidation, with no subsequent deprotonation. The result is a cationic histidine (Scheme 1A). The second involves histidine accepting a proton and subsequently deprotonating to produce a neutral histidine (Scheme 1B). It is important to note that, in Scheme 1B, the histidine must deprotonate from its π-nitrogen, if His189 is to act as a proton donor to tyrosine upon reduction.

Scheme 1

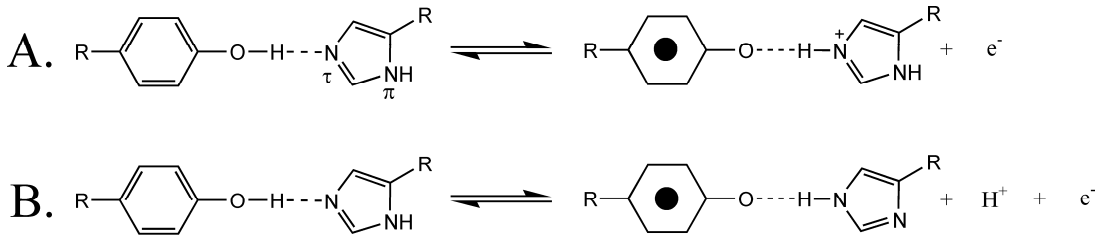

In previous work (Chapter 3), we have identified an additional $Y_D^{\bullet}$ proton donation pathway besides His189. We have proposed that this second proton donation pathway is His189D2 (Figure 1A, pathway 1) and a chain of water molecules (Figure 1B, pathway 2). The implication is that the PCET mechanism for $Y_D^{\bullet}$ decay may be more complex than the previously proposed rocking mechanism of Scheme 1, at least at alkaline pH. Furthermore, in this multipathway model, the relative population of each pathway may be influenced by changing the pH of the surrounding media.

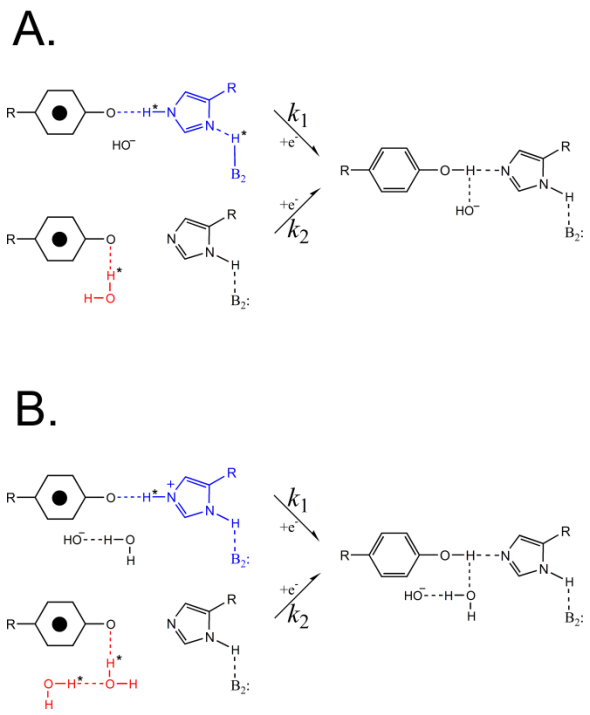

Figure 1. Schematic of proton donation pathways for $Y_D^{\bullet}$. The asterisks indicate the protons in motion. A. In pathway 1, histidine (blue) is involved in the multiproton pathway. In pathway 2, a water molecule (red) is proposed to act as a single proton donor. B. In pathway 1, histidine (blue) is proposed to act as a single proton donor. In pathway 2, a chain of water molecules (red) are involved in the multiproton pathway.

In order to further elucidate the mechanism of $Y_D^{\bullet}$ decay and to help determine how the surrounding environments for $Y_D^{\bullet}$ and $Y_Z^{\bullet}$ are influenced by pH, we have studied the pH dependence of the EPR g-tensors (Figure 2). The g_x component of the g-tensor is an excellent probe of the environment surrounding tyrosyl radicals, as it is particularly sensitive to hydrogen bonding and localized electrostatic effects.[11-18]

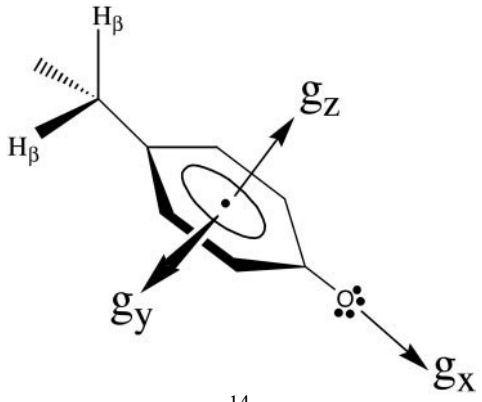

Figure 2. Orientation of tyrosine g-tensors.[14]

4.3 Materials and Methods

PSII was isolated from market spinach.[19] The oxygen evolution rates were > 600 μmol O_2/(mg chl h)$^{-1}$.[20] PSII was depleted of the OEC, as well as the 18-, 24- and 33-kDa extrinsic polypeptides, by treatment with Tris buffer (final concentration, 0.8 M Tris-HCl and 2.0 mM tetrasodium EDTA) at pH 8.0.[21] The PSII samples were stored in pH 6.0 buffer (0.40 M sucrose, 50 mM MES-NaOH, 15 mM NaCl) at -70 ºC. Multiple lots of the Tris-treated PSII samples were made in this manner, and all lots were pooled before buffer exchange.

The Tris-treated PSII samples were buffer exchanged into pH 5.0, 5.5, 6.0 and 8.0 media. The pL 5.0 and 5.5 samples were exchanged into a buffer containing 0.40 M sucrose, 50 mM succinic acid-NaOH and 15 mM NaCl. The pH 6.0 sample was exchanged into a buffer containing 0.40 M sucrose, 50 mM MES-NaOH and 15 mM NaCl. The pH 8.0 sample was exchanged into a buffer containing 0.40 M sucrose, 50 mM HEPES-NaOH and 15 mM NaCl. Buffer exchange at each pH value was begun by homogenizing 4.0 mL of the Tris-treated sample, which was stored in pH 6.0 buffer. The sample was then centrifuged at 50,000 x *g* for 5 min. and the supernatant decanted. The

pellet was next resuspended into 4.0 mL of the selected exchange buffer and homogenized. The resuspended sample was again centrifuged at 50,000 x *g* for 5 min. and the supernatant decanted. This procedure was repeated two additional times, for a total of three resuspensions. After buffer exchange, the samples were stored at -70 ºC in 250 µL aliquots until use.

The EPR experiments were conducted using a home-built continuous wave/pulsed D-band (130 GHz) EPR spectrometer. The microwave bridge was constructed by Dr. V. N. Krymov. A cylindrical TE_{011} cavity was employed. This cavity has several slits to allow for optical excitation and magnetic field modulation. The maximum power output in the pulsed mode is 125 mW and 3.4 mW in continuous wave mode. For the light excitation of the sample, an Opotek (Carlsbad, CA) optical parametric oscillator (Carlsbad, CA) pumped by a Quantel (Evry, France) Nd:YAG laser was used. The power was < 1 mJ. The output of the laser was coupled to an optical fiber, which terminates near the illumination slits in the cavity. The temperature was controlled by an Oxford (Oxon, UK) temperature control system coupled to an Oxford flow cryostat.

Each sample contained 3.0 mM potassium ferricyanide as an electron acceptor and 3.0 mM potassium ferrocyanide as an electron donor. After addition of ferricyanide and ferrocyanide, the samples were concentrated by centrifugation at 16,000 x *g* for 15 min. at 4 ºC. The concentrated samples were loaded into quartz tubes having an i.d. of 0.45 mm and an o.d. of 0.55 mm. For the dark adapted samples, the samples were pre-illuminated in the resonant cavity with 30 pulses of 532 nm light at 10 Hz. The samples were then dark adapted for 10 s and then frozen to 40 K. For the light samples, the sample was illuminated with approximately 30 pulses of 532 nm light at 10 Hz as it was

cooled to 40 K. Spectra were recorded at 40 K. The power was attenuated at 50 dB. The magnetic field modulation was 1.5 G. All data were smoothed by two applications of a binomial algorithm.

Spectra for $Y_Z^{\bullet}$ were obtained by subtracting the dark adapted spectra from the spectra obtained under illumination at each pH value. The dark adapted sample contains the spectrum for $Y_D^{\bullet}$, whereas the illuminated sample contains contributions from both $Y_D^{\bullet}$ and $Y_Z^{\bullet}$. The light-minus-dark component corresponds to $Y_Z^{\bullet}$.

4.4 Results

In Figure 3, we present the high field EPR spectrum of $Y_D^{\bullet}$ measured as a function of pH. The data shows that the g_x component for $Y_D^{\bullet}$ is 2.0076 and is pH independent from 5.5-8.0. The value of the g_y component is 2.0043. The value of the g_z component is 2.0022. Both the g_y component and the g_z component are also pH independent. The weak signal at pH 5.0 makes the determination of the g-tensor components difficult, but there are no major changes when compared with the samples from pH 5.5-6.0.

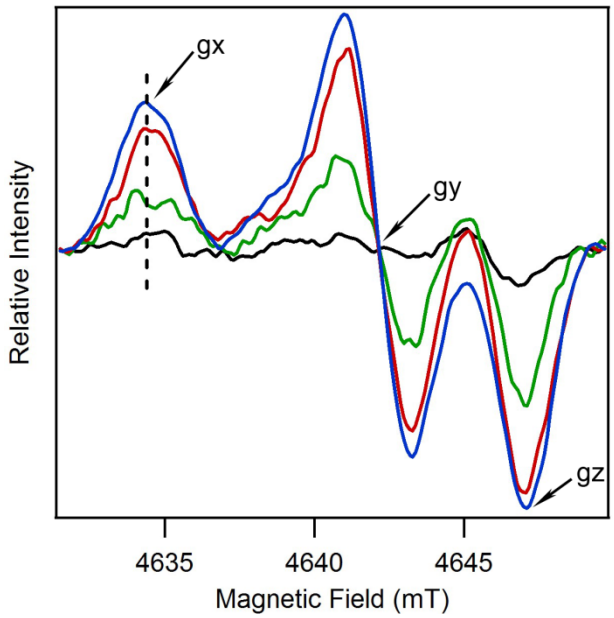

Figure 3. 130 GHz EPR spectra of $Y_D^{\bullet}$ from pH 5.0-8.0, showing g_x component invariance as a function of pH. The position of the g-tensor components is also indicated. The dashed black line is at g = 2.0076. The g_y component = 2.0043. The g_z component = 2.0022. The pH for the individual traces are as follows: blue = pH 8.0; red = pH 6.0; green = pH 5.5; black = pH 5.0.

In Figure 4, we present the high field EPR spectrum of $Y_Z^{\bullet}$ measured as a function of pH. The width of the g_x component is 0.0022 g. This broad, weak $Y_Z^{\bullet}$ g_x component is in agreement with previously reported work in a Y_D site-directed mutant (~ 0.0024).[11] As shown in figure 4, the g_x component was found to decrease upon increasing pH. These values are reported in Table 1. The value of the g_y component is 2.0044. The value of the g_z component is 2.0022. Again, both the g_y component and the g_z component are pH independent.

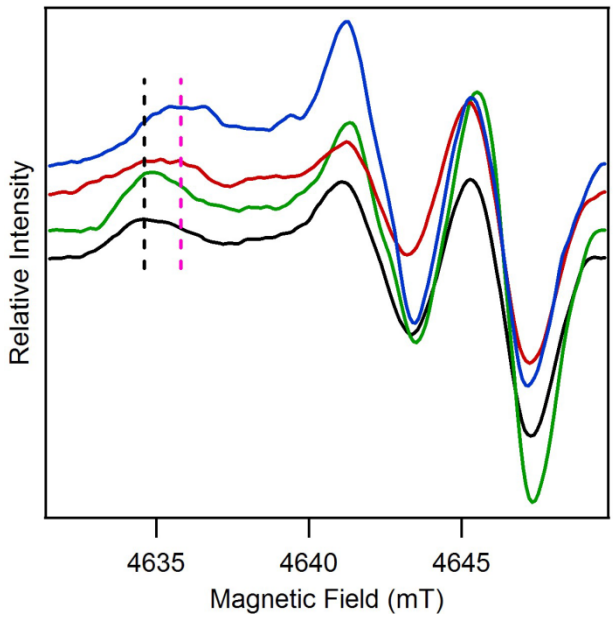

Figure 4. 130 GHz EPR spectra of $Y_Z^{\bullet}$ from pH 5.0-8.0, showing the pH dependence of the g-tensor. The dashed black line is at g = 2.0076. The dashed pink line is at g = 2.0071. The spectrum was obtained by a light-minus-dark subtraction. The g_y component = 2.0044. The g_z component = 2.0022. The pH for the individual traces are as follows: blue = pH 8.0; red = pH 6.0; green = pH 5.5; black = pH 5.0.

Table 1. The pH dependence of the g_x component of $Y_Z^{\bullet}$, as derived from Figure 4.

pH	5.0	5.5	6.0	8.0
g_x	2.0076	2.0074	2.0073	2.0071

4.5 Discussion

The tyrosyl radical g-tensor is known to be sensitive to the surrounding environment. The g_y and g_z components are not usually altered,[11-18] while the g_x component is particularly sensitive to hydrogen bonding, as it is aligned along the phenol C-O bond (Figure 2).[12,14,18] The g_x component can be affected by the protonation state,

distance and angle of the hydrogen bonding pair.[12,13,18] More electropositive environments, such as stronger hydrogen bonds, decrease the g_x component.[11-15,18] Altering the hydrogen bond angle from a linear to bent configuration has given more ambiguous results,[12,13] but orientations that increase hydrogen bond strength will likely decrease the g_x component. For example, g_x components have been reported with values between 2.0094[17] and 2.0064[14], depending on the hydrogen bonding state of the tyrosyl radical. Non-hydrogen bonded neutral tyrosyl radicals have reported g_x component values of 2.0088 ± 0.0004.[11,17,18,22-24] Neutral tyrosyl radicals, when hydrogen bonded to a neutral species, have g_x components of 2.0075 ± 0.0002.[11,14,18,25-29] Neutral phenoxyl radicals, when hydrogen bonded to a cationic species, have reported g_x components of 2.0065 ± 0.0002.[14,17,30] Finally, non-hydrogen bonded cationic phenoxyl g_x components have been calculated to be approximately 2.0040 ± 0.0005, but have not been experimentally detected.[12,31]

The $Y_D^{\bullet}$ data in Figure 3 help to assess whether His189 is a cationic or neutral species (Scheme 1). If Scheme 1A is operational, then we would expect to see a g_x component of approximately 2.0065 due to the cationic histidine. In contrast, if Scheme 1B is operational, then we would expect to see a g_x component near 2.0075, as the histidine would be a neutral species. EPR spectroscopy at 130 GHz is able to provide the necessary resolution, as our instrument under these conditions has a resolution > 0.0001 g.

We do not observe a g_x component at 2.0065 in our $Y_D^{\bullet}$ data (Figure 3), which would suggest a cationic imidazole. Therefore, the data may be consistent with a hydrogen bond between $Y_D^{\bullet}$ and a neutral His189D2 species throughout the range

examined. Histidine may be able to remain neutral from pH 5.0-8.0 by deprotonation, via resonance, from the π-nitrogen of histidine to an unidentified base (Scheme 1B). This is consistent with the transfer of more than one proton in the rate-limiting step of $Y_D^{\bullet}$ reduction, as previously proposed (Chapter 3).

Figure 3 also shows that only one g_x component is observed throughout the pH range. The observance of two peaks would be consistent with a hydrogen bond from a second species, possibly the proton donor from the second proton donation pathway (Figure 1, pathway 2). However, the absence of two g_x components is not in contradiction to the existence of the two proton donation pathway model because the g_x component may be overlapping or one proton donor may not be hydrogen bonding (or only weakly so).

Examining Figure 4 and Table 1, we observe that the environment surrounding $Y_Z^{\bullet}$ becomes more electropositive with increasing pH. The pH dependence of the g_x component is probably not due to the protonation of the hydrogen bonding partner of $Y_Z^{\bullet}$. We would not expect the hydrogen bond partner to become protonated as the conditions become more alkaline. It is more likely that the environment around $Y_Z^{\bullet}$ becomes more electropositive due to changes in hydrogen bonding. This could occur through a reduction in the hydrogen bond length between the radical and its hydrogen bonding partner, a change in orientation between the hydrogen bonding partners, or the acquisition of more hydrogen bonding partners at higher pH. Despite the change in the g_x component values, the g_x components observed in Figure 4 (2.0076 to 2.0071) are suggestive of a hydrogen bond to a neutral species throughout the pH range examined.

An empirical model has been developed that relates the value of the g_x component to the hydrogen bonding distance in angstroms: $g_x = 2.0094 - 0.0033/(r - 0.5)^2$, where r is the hydrogen bond distance.[11] Using this model, we can calculate that $Y_Z^{\bullet}$ is 1.85 Å from its hydrogen bonding partner at pH 5.0 and 1.70 Å away at pH 8.0. This calculation illustrates that small changes in hydrogen bonding may be able to explain the differences in $Y_Z^{\bullet}$ g_x components over the pH range of 5.0-8.0.

A similar effect has been observed with the tyrosyl radical g_x component of catalase.[15] In that work, Ivancich et al. observed g_x components of 2.00740 at pH 6.7 for the tyrosyl radical. When the pH decreased to 4.5, the g_x component increased to 2.00760. The authors also reasoned that there was a strengthening of the hydrogen bond to the tyrosyl radical at the higher pH value.

It is also possible that the change in g_x component observed for $Y_Z^{\bullet}$ from pH 5.0-8.0 may be a result of our subtraction procedure. At pH 6.0 to 8.0, the half-life for $Y_D^{\bullet}$ is greater than 19 min. (see Chapter 3 and ref [32]), so we believe our subtraction spectra should have minimal contributions from $Y_D^{\bullet}$ in this pH range. However, at pH $\leq$ 5.5 the decay rate begins to increase dramatically. For example, the estimated half-life for $Y_D^{\bullet}$ at pH 5.0 is on the order of one minute.[32] Therefore, substantial contributions from $Y_D^{\bullet}$ may be present in the light-minus-dark spectra (Figure 4) for pH $\leq$ 5.5, given our 10 s dark adaptation procedure. Additional experiments are in progress to address this point.

In conclusion, high field EPR spectroscopy suggests that both $Y_D^{\bullet}$ and $Y_Z^{\bullet}$ are hydrogen bonded to neutral species. We do not observe the presence of multiple g_x components for $Y_D^{\bullet}$, which would indicate the presence of a second hydrogen bond donor to $Y_D^{\bullet}$; however, the g_x component for the two proton donors could be overlapping or one

species is not hydrogen bonding. The environment surrounding $Y_Z^{\bullet}$ becomes more electropositive as the pH is increased from pH 5.0-8.0. We attribute this to a pH induced change in hydrogen bond distance, to a change in orientation, or to an increase in the number of hydrogen bonding partners. In contrast, the environment of $Y_D^{\bullet}$ seems to vary little from pH 5.0-8.0. This may be due to compensating changes from multiple proton donation pathways. The lack of a peak at g = 2.0065 in Figure 3, which would indicate the presence of a cationic imidazole, suggests that His189 may deprotonate from its π-nitrogen upon Y_D oxidation, consistent with multiple protons being transferred in the rate-limiting step.

4.6 Acknowledgment

This work was supported by the National Institutes of Health, GM43273 (B. A. B.).

4.7 References

(1) Biesiadka, J.; Loll, B.; Kern, J.; Irrgang, K.-D.; Zouni, A. Crystal structure of cyanobacterial photosystem II at 3.2 Å resolution: a closer look at the Mn-cluster. *Phys. Chem. Chem. Phys.* **2004**, *20*, 4733-4736.

(2) Ferreira, K. N.; Iverson, T. M.; Maghlaoui, K.; Barber, J.; Iwata, S. Architecture of the photosynthetic oxygen-evolving center. *Science* **2004**, *303*, 1831-1837.

(3) Guskov, A.; Kern, J.; Gabdulkhakov, A.; Broser, M.; Zouni, A.; Saenger, W. Cyanobacterial photosystem II at 2.9- Å resolution and the role of quinones, lipids, channels and chloride. *Nat. Struct. Mol. Biol.* **2009**, *16*, 334-342.

(4) Loll, B.; Kern, J.; Saenger, W.; Zouni, A.; Biesiadka, J. Towards complete cofactor arrangement in the 3.0 Å resolution structure of photosystem II. *Nature* **2005**, *438*, 1040-1044.

(5) Debus, R. J.; Barry, B. A.; Babcock, G. T.; McIntosh, L. Site-specific mutagenesis identifies a tyrosine radical involved in the photosynthetic oxygen-evolving complex. *Proc. Natl. Acad. Sci. USA* **1988**, *85*, 427-430.

(6) Debus, R. J.; Barry, B. A.; Sithole, I.; Babcock, G. T.; McIntosh, L. Directed mutagenesis indicates that the donor to P_{680}^{+} in photosystem II is Tyr-161 of the D1 polypeptide. *Biochemistry* **1988**, *27*, 9071-9074.

(7) Babcock, G. T.; Barry, B. A.; Debus, R. J.; Hoganson, C. W.; Atamian, M.; McIntosh, L.; Sithole, I.; Yocum, C. F. Water oxidation in photosystem II: From radical chemistry to multielectron chemistry. *Biochemistry* **1989**, *28*, 9557-9565.

(8) Campbell, K. A.; Peloquin, J. M.; Diner, B. A.; Tang, X.-S.; Chisholm, D. A.; Britt, R. D. The τ-Nitrogen of D2 histidine 189 is the hydrogen bond donor to the tyrosine radical $Y_D^{\bullet}$ of photosystem II. *J. Am. Chem. Soc.* **1997**, *119*, 4787-4788.

(9) Force, D. A.; Randall, D. W.; Britt, R. D.; Tang, X.-S.; Diner, B. A. ^{2}H ESE-ENDOR study of hydrogen bonding to the tyrosine radicals $Y_D^{\bullet}$ and $Y_Z^{\bullet}$ of photosystem II. *J. Am. Chem. Soc.* **1995**, *117*, 12643-12644.

(10) Mino, H.; Kawamori, A. Microenvironments of Tyrosine D^{+} and Tyrosine Z^{+} in photosystem II studied by proton matrix ENDOR. *Biochim. Biophys. Acta* **1994**, *1185*, 213-220.

(11) Un, S.; Tang, X.-S.; Diner, B. A. 245 GHz High-field EPR study of tyrosine-$D^{\bullet}$ and Tyrosine-$Z^{\bullet}$ in mutants of photosystem II. *Biochemistry* **1996**, *35*, 679-684.

(12) Brynda, M.; Britt, R. D. Density Functional Theory calculations on the magnetic properties of the model tyrosine radical-histidine complex mimicking tyrosyl radical $Y_D^{\bullet}$ in Photosystem II. *Res. Chem. Intermed.* **2007**, *33*, 863-883.

(13) Engstrom, M.; Himo, F.; Graslund, A.; Minaev, B.; Vahtras, O.; Agren, H. Hydrogen bonding to tyrosyl radical analyzed by ab initio g-tensor calculations. *J. Phys. Chem. A* **2000**, *104*, 5149-5133.

(14) Faller, P.; Goussias, C.; Rutherford, A. W.; Un, S. Resolving intermediates in biological proton-coupled electron transfer: A tyrosyl radical prior to proton movement. *Proc. Natl. Acad. Sci. USA* **2003**, *100*, 8732-8735.

(15) Ivancich, A.; Mattioli, T. A.; Un, S. Effect of protein microenvironment on tyrosyl radicals. A high-field (285 GHz) EPR, resonance raman, and hybrid density functional study. *J. Am. Chem. Soc.* **1999**, *121*, 5743-5753.

(16) Liu, A. M.; Barra, A. L.; Rubin, H.; Lu, G. Z.; Graslund, A. Heterogeneity of the local electrostatic environment of the tyrosyl radical in *Mycobacterium tuberculosis* ribonucleotide reductase observed by high-field electron paramagnetic resonance. *J. Am. Chem. Soc.* **2000**, *122*, 1974-1978.

(17) Mezzetti, A.; Maniero, A. L.; Brustolon, M.; Giacometti, G.; Brunel, L. C. A tyrosyl radical in an irradiated single crystal of N-acetyl-L-tyrosine studied by X-band cw-EPR, high-frequency EPR, and ENDOR spectroscopies. *J. Phys. Chem. A* **1999**, *103*, 9636-9643.

(18) Un, S.; Atta, M.; Fontecave, M.; Rutherford, A. W. g-Values as a probe of the local protein environment: High-field EPR of tyrosyl radicals in ribonucleotide reductase and photosystem II *J. Am. Chem. Soc.* **1995**, *117*, 10713-10719.

(19) Berthold, D. A.; Babcock, G. T.; Yocum, C. F. A highly resolved, oxygen-evolving Photosystem II preparation from spinach thylakoid membranes. *FEBS Lett.* **1981**, *134*, 231-234.

(20) Barry, B. A. Tyrosyl radicals in photosystem II. *Methods Enzymol.* **1995**, *258*, 303-319.

(21) Yamomoto, Y.; Doi, M.; Tamura, N.; Nishimura, N. Release of polypeptides from highly active O_2-evolving photosystem II preparation by Tris treatment. *FEBS Lett.* **1981**, *133*, 265-268.

(22) Allard, P.; Barra, A. L.; Andersson, K. K.; Schmidt, P. P.; Atta, M.; Graslund, A. Characterization of a new tyrosyl free radical in *Salmonella typhimurium* ribonucleotide reductase with EPR at 9.45 and 245 GHz. *J. Am. Chem. Soc.* **1996**, *118*, 895-896.

(23) Gerfen, G. J.; Bellew, B. F.; Un, S.; Bollinger, J. M.; Stubbe, J.; Griffin, R. G.; Singel, D. J. High-frequency (139.5 GHz) EPR spectroscopy of the tyrosyl radical in *Escherichia coli* ribonucleotide reductase. *J. Am. Chem. Soc.* **1993**, *115*, 6420-6421.

(24) Hoganson, C. W.; Sahlin, M.; Sjoberg, B. M.; Babcock, G. T. Electron magnetic resonance of the tyrosyl radical in ribonucleotide reductase from *Escherichia coli*. *J. Am. Chem. Soc.* **1996**, *118*, 4672-4679.

(25) Dorlet, P.; Rutherford, A. W.; Un, S. Orientation of the tyrosyl D, pheophytin anion, and semiquinone $Q_A^{\bullet-}$ radicals in photosystem II determined by high-field electron paramagnetic resonance. *Biochemistry* **2000**, *39*, 7826-7834.

(26) Hofbauer, W.; Zouni, A.; Bittl, R.; Kern, J.; Orth, P.; Lendzian, F.; Fromme, P.; Witt, H. T.; Lubitz, W. Photosystem II single crystals studied by EPR spectroscopy at 94 GHz: The tyrosine radical $Y_D^{\bullet}$. *Proc. Natl. Acad. Sci. USA* **2001**, *98*, 6623-6628.

(27) Gulin, V. I.; Dikanov, S. A.; Tsvetkov, Y. D.; Evelo, R. G.; Hoff, A. J. Very high frequency (135 GHz) EPR of the oxidized primary donor of the photosynthetic bactria *Rb. sphaeroides* R-26 and *Rps. viridis* and of $Y_D^{\bullet}$ (signal II) of plant photosystem II. *Pure Appl. Chem.* **1992**, *64*, 903-906.

(28) van Dam, P. J.; Willems, J. P.; Schmidt, P. P.; Potsch, S.; Barra, A. L.; Hagen, W. R.; Hoffman, B. M.; Andersson, K. K.; Graslund, A. High-frequency EPR and pulsed Q-Band ENDOR studies on the origin of the hydrogen bond in tyrosyl radicals of ribonucleotide reductase R2 proteins from mouse and herpes simplex virus type 1. *J. Am. Chem. Soc.* **1998**, *120*, 5080-5085.

(29) Farrar, C. T.; Gerfen, G. J.; Griffin, R. G.; Force, D. A.; Britt, R. D. Electronic structure of the Y-D tyrosyl radical in photosystem II: A high-frequency electron paramagnetic resonance spectroscopic and density functional theoretical study. *J. Phys. Chem. B* **1997**, *101*, 6634-6641.

(30) Fasanella, E.; Gordy, W. Electron spin resonance of an irradiated single crystal of L-tyrosine HCl. *Proc. Natl. Acad. Sci. USA* **1969**, *62*, 299-304.

(31) Benisvy, L.; Bittl, R.; Bothe, E.; Garner, C. D.; McMaster, J.; Ross, S.; Teutloff, C.; Neese, F. Phenoxyl radicals hydrogen-bonded to imidazolium: Analogues of tyrosyl D of photosystem II: High-field EPR and DFT studies. *Angew. Chem. Int. Ed.* **2005**, *44*, 5314-5317.

(32) Jenson, D. L.; Evans, A.; Barry, B. A. Proton-coupled electron transfer and tyrosine D of photosystem II. *J. Phys. Chem. B* **2007**, *111*, 12599-12604.

Conclusion

I have used EPR spectroscopy and isotopic substitution to gain increased knowledge about the PCET mechanism for $Y_D^{\bullet}$ reduction. First, I examined the pL dependence of both the rate constant and kinetic isotope effect for $Y_D^{\bullet}$ reduction. Second, I examined the manner in which protons are transferred during the rate-limiting step for $Y_D^{\bullet}$ reduction at alkaline pL. Finally, I examined the effect of pH on the environment surrounding both $Y_D^{\bullet}$ and $Y_Z^{\bullet}$.

I determined, through an analysis of solvent kinetic isotope effects, that the PCET decay mechanism for $Y_D^{\bullet}$ is pL dependant. At pL $\geq$ 7.5, my data are consistent with the reduction of $Y_D^{\bullet}$ through a coupled proton-electron transfer (CPET) mechanism. In the CPET mechanism, both the proton and the electron are transferred in the rate-limiting step. I was able to assign the CPET mechanism based on the significant kinetic isotope effects observed at alkaline pL. My data also indicate that a proton transfer-electron transfer (PTET) mechanism occurs at acidic pL. In the PTET mechanism, the proton is transferred first in a pre-equilibrium step, followed by electron transfer.

I conducted a proton inventory experiment to examine the effect of mixed ^1H_2O:^2H_2O solutions on the decay rate of $Y_D^{\bullet}$ at pL 8.0. The proton inventory experiment is able to identify the number of protons transferred in the rate-limiting step by utilizing derivations of the Gross-Butler equation. Through the use of proton inventory, I was able to determine that the proton transfer mechanism is more complex than the previously proposed. My results indicate that there is more than one proton donation pathway to $Y_D^{\bullet}$ during reduction and that one of those pathways must involve

multiple protons. I proposed that these two pathways include histidine and a chain of water molecules.

My high-field EPR studies suggest that the hydrogen bonding environment surrounding $Y_D^{\bullet}$ changes little throughout the range pH 5.0-8.0. Additionally, the lack of an EPR g_x component at 2.0065 implies that the imidazole hydrogen bonding partner to $Y_D^{\bullet}$ is neutral. This result indicates that His189 of the D2 polypeptide may be able to deprotonate, through resonance, from its π-nitrogen. This is consistent with the finding that more than one proton is transferred in the rate-limiting step during $Y_D^{\bullet}$ reduction.

Finally, I have also determined that the environment of $Y_Z^{\bullet}$ does change as a function of pH. The environment of $Y_Z^{\bullet}$ becomes more electropositive with increasing pH. Because it is unlikely that the proton acceptor to $Y_Z^{\bullet}$ becomes protonated as the pH becomes more alkaline, I proposed that the environment becomes more electropositive through a change in hydrogen bond strength. This could occur through a change in hydrogen bond length, a change in hydrogen bond orientation, or an increase in the number of hydrogen bonding partners to $Y_Z^{\bullet}$ as the pH is increased.

Future Directions

The following experiments would be beneficial for to acquire further understanding of $Y_D^{\bullet}$ PCET reduction mechanisms in photosystem II:

1) $^1H_2{}^{17}O$ ESE-ENDOR spectroscopy. The identification of water as a hydrogen bond donor to $Y_D^{\bullet}$ would reinforce the conclusion of multiple proton donors to $Y_D^{\bullet}$.

2) pL dependence and proton inventory of $Y_Z^{\bullet}$. While $Y_D^{\bullet}$ and $Y_Z^{\bullet}$ have a similar symmetric arraignment in photosystem II, their roles in the enzyme are quite different. A comparison of redox chemistry between the two tyrosyl radicals would help to explain how protein environment alters the PCET reduction dynamics of redox active amino acids.

3) Determination of the protonation state of His189D2 when Y_D is in the reduced state. The steady state yield of $Y_D^{\bullet}$ is low below approximately pL 5.5-6.0. It is unknown whether this is due to the unavailability of His189D2 as a proton acceptor due to protonation, or if others factors are involved. To construct a proper model for Y_D PCET redox chemistry, the protonation state of His189D2 must be known when Y_D is in the reduced state. Infrared spectroscopy or resonance Raman spectroscopy would both be suitable techniques, as long as the signal-to-noise level permits.

Appendix 1

Copyright Permission for Chapter 2

AMERICAN CHEMICAL SOCIETY LICENSE TERMS AND CONDITIONS

Feb 11, 2009

This is a License Agreement between David L Jenson ("You") and American Chemical Society ("American Chemical Society") provided by Copyright Clearance Center ("CCC"). The license consists of your order details, the terms and conditions provided by American Chemical Society, and the payment terms and conditions.

All payments must be made in full to CCC. For payment instructions, please see information listed at the bottom of this form.

License Number	2126090421712
License date	Feb 11, 2009
Licensed content publisher	American Chemical Society
Licensed content publication	The Journal of Physical Chemistry B
Licensed content title	Proton-Coupled Electron Transfer and Tyrosine D of Photosystem II
Licensed content author	David L. Jenson , Amaris Evans , and Bridgette A. Barry*
Licensed content date	Nov 1, 2007
Volume number	111
Issue number	43
Type of Use	Thesis/Dissertation
Requestor type	Not specified
Format	Print
Portion	Full article
Author of this ACS article	Yes
Order reference number	
Title of the thesis / dissertation	Proton-Coupled Electron Transfer and Tyrosine D of Photosystem II
Expected completion date	Apr 2009
Estimated size(pages)	125
Billing Type	Invoice
Billing Address	389 Calhoun St. #2 Atlanta, GA 30318 United States
Customer reference info	
Total	0.00 USD
Terms and Conditions	

Thesis/Dissertation